Manuscript prepared for Atmos. Chem. Phys.
with version 2015/09/17 7.94 Copernicus papers of the LaTeX class copernicus.cls.
Date: 6 June 2016

Upper tropospheric CO and O3 budget during the Asian Summer Monsoon

B. Barret[1,2], B. Sauvage[1,2], Y. Bennouna[1,2], and E. Le Flochmoen[1,2]

[1]Laboratoire d'Aérologie/OMP, Université de Toulouse, Toulouse, France.
[2]CNRS UMR 5560, 14 avenue E. Belin, 31400 Toulouse, France.

Correspondence to: Barret Brice
(brice.barret@aero.obs-mip.fr)

Abstract. During the Asian Summer Monsoon, the circulation in the Upper Troposphere-Lower Stratosphere (UTLS) is dominated by the Asian Monsoon Anticyclone (AMA). Pollutants convectively uplifted to the upper troposphere are trapped within this anticyclonic circulation that extends from the Pacific Ocean to the eastern Mediterranean basin. Among the uplifted pollutants are ozone (O_3) and its precursors, such as carbon monoxide (CO) and nitrogen oxides (NOx). Many studies based on global modelisation and satellite data have documented the source regions and transport pathways of primary pollutants (CO, HCN) into the AMA. Here, we aim to quantify the O_3 budget by taking into consideration anthropogenic and natural sources. We first use CO and O_3 data from the Metop-A/IASI sensor to document their tropospheric distributions over Asia, taking advantage of the useful information they provide on the vertical dimension. These satellite data are used together with MOZAIC tropospheric profiles recorded in India to validate the distributions simulated by the global GEOS-Chem chemistry transport model. Over the Asian region, UTLS monthly CO and O_3 distributions from IASI and GEOS-Chem display the same large-scale features. UTLS CO columns from GEOS-Chem are in agreement with IASI, with a low bias of $11\pm9\%$ and a correlation coefficient of 0.70. For O_3, the model underestimates IASI UTLS columns over Asia by $14\pm26\%$ but the correlation between both is high (0.94). GEOS-Chem is further used to quantify the CO and O_3 budget through sensitivity simulations. For CO, these simulations confirm that South-Asian anthropogenic emissions have a more important impact on enhanced concentrations within the AMA ($\sim$25 ppbv) than East-Asian emissions ($\sim$10 ppbv). The correlation between enhanced emissions over the Indo-gangetic-Plain and monsoon deep convection is responsible for this larger impact. Consistently, South-Asian anthropogenic NOx emissions also play a larger role in producing O_3 within the AMA ($\sim$8 ppbv) than East-Asian emissions ($\sim$5 ppbv) but Asian lightning produced NOx are responsible for the largest O_3 production (10-14 ppbv). Stratosphere to Troposphere Exchanges (STE) are also important in transporting O_3 in the upper part of the AMA.

1 Introduction

Tropospheric O_3 plays an important role in determining the radiative budget of the atmosphere and has a non-negligible impact on climate change. In particular, according to Shindell et al. (2006), the fast economic growth of developing countries has led to an increase in tropospheric O_3 which may be responsible for the fast warming observed in the tropics over the latest half of the 20th century. Based on GCM simulations, Chen et al. (2007) have also shown that the changes in tropospheric O_3 predicted for the 21st century are likely to increase the atmospheric radiative forcing throughout the troposphere but more specifically in the tropical Upper Troposphere-Lower Stratosphere (UTLS). The understanding of the O_3 budget in this atmospheric region is therefore an important issue to better address future tropospheric O_3 radiative forcing.

During boreal summer, the northern-hemisphere tropical tropospheric circulation is dominated by the Asian Summer Monsoon (ASM), which is characterized by a strong south-westerly flow in the lower troposphere converging over south and south-east Asia and results in deep convective activity over this region. During the ASM, an upper level anticyclonic circulation, the Asian Monsoon Anticyclone (AMA), builds up in response to deep convection (Hoskins and Rodwell, 1995; Garny and Randel, 2013). Based on CO UTLS data provided by the Aura/MLS (Microwave Limb Sensor) sensor, Li et al. (2005); Park et al. (2007); Barret et al. (2008) have shown that during the ASM, polluted air-masses were convectively uplifted to the UTLS and trapped within AMA circulation. Based on ACE-FTS data, Park et al. (2008) have also pointed out that similarly to CO, HCN is trapped within the AMA. Randel et al. (2010) have further highlighted that HCN from the AMA is uplifted into the stratosphere within the ascending branch of the Brewer-Dobson circulation. Data from the AIRS sensor were also used to show that the uplift of O_3-poor and H_2O rich air masses from the Planetary Boundary Layer (PBL) is responsible for low O_3 within the AMA (Randel and Park, 2006). The AMA therefore appears to be an isolated atmospheric region with its physical properties and its composition likely little impacted by emissions and processes from remote regions.

Recent studies based on transport modeling have tried to determine the origin of the air masses convectively uplifted and trapped within the AMA. For instance, based on Lagrangian dispersion modeling forced with a set of reanalyzes from different systems, Bergman et al. (2013) argue that PBL air masses impacting the AMA are uplifted within a conduit centered over Northeastern India, Nepal and southern Tibet. Using high resolution WRF meteorological forcing for back trajectory simulations, Heath and Fuelberg (2014) have demonstrated that most of the air parcels convectively uplifted from the PBL and ending up in the AMA at 100 hPa originate in the Tibetan Plateau or the Himalayan southern slopes. Nevertheless, these studies based on Lagrangian modeling are not able to document the origin of pollutants in the AMA, which depends on the distribution of their sources. It is noteworthy that convection from the Tibetan Plateau, highlighted as predominant to fill

the AMA by the cited studies (Bergman et al., 2013; Heath and Fuelberg, 2014), probably plays a minor role in the transport of pollutants due to its very low pollution sources. From simulations with a global Chemistry Transport Model (CTM), Park et al. (2009) have highlighted that most of the CO trapped within the AMA at 100 hPa comes from India and Southeast Asia and to a lesser extent from Eastern China. A more recent study based on similar simulations with the WRF-Chem limited area model comes to similar conclusions (Yan and Bian, 2015). According to Park et al. (2009), almost no CO originates from the Tibetan Plateau. Also based on CTM simulations, Li et al. (2005) point to North-East India and South-West China as the origin of upper tropospheric CO trapped within the AMA.

Based on CTM sensitivity simulations, Kunhikrishnan et al. (2004) have quantified the impact of surface NOx from India and the neighboring regions on the O_3 budget over India. Their results show that O_3 in the Indian middle-upper troposphere (500-150 hPa) during the monsoon is mostly produced by regional (Indian) NOx emissions uplifted by convection. In particular, they point to a larger impact of NOx local surface sources relative to the lightning produced NOx (LiNOx) source on the NOx concentration in the 500-150 hPa layer during the monsoon. Based on in-situ data recorded at the Himalayan NCO-P observatory, Cristofanelli et al. (2010) have shown that high altitude **(5049 m a.s.l.)** O_3 has a marked seasonal cycle with a maximum of around 60 ppbv during the pre-monsoon season and a minimum of 40 ppbv during the monsoon season. They show that this annual cycle is largely related to Stratosphere to Troposphere Exchanges (STE) which occur about 20% of the time all year round except during the monsoon season. During the October-May period, the Subtropical Westerly Jet (SWJ) is located between 25°N and 30°N promoting deep STE over the southern Himalayas. During the ASM, the SWJ is pushed northwards of the Tibetan Plateau by the AMA, and STE to the central Himalayas are blocked.

Previous studies (Kunhikrishnan et al., 2004, 2006) have therefore dealt with the O_3 budget in the Indian troposphere, but the O_3 budget of the AMA has not yet been addressed in detail. In particular, it is not yet known to what extent the different NOx sources are responsible for an increase in the O_3 concentrations within this upper level large scale circulation characterized by rather low O_3 concentrations. Furthermore, satellite data from the IASI sensor have been available since 2007 but they have not yet been used to document the ASM. These data are complementary to MLS data that have been extensively used in the region (Park et al., 2009; Barret et al., 2008) because, although they have a coarse vertical resolution, they cover both the troposphere and the UTLS. Here, we aim to characterize the impact of STE and of NOx emissions from the different sources and regions on the O_3 budget in the south Asian UTLS during the monsoon season. We also use CO as a tracer of surface pollution that brings direct information about the origin of the air masses. We focus on the AMA in order to determine the role of its dynamical structure and isolation upon the regional

upper tropospheric O_3 budget. The second section of this paper is dedicated to the description of the observations (IASI and MOZAIC) and of the chemistry transport model GEOS-Chem (GC) that are used in our study. In section 3, we make use of IASI and MOZAIC O_3 and CO data to validate their distributions simulated by the GC model over Asia. In section 4, we discuss the dynamical and chemical characteristics of the AMA and the role of convection in controlling the distributions of CO and O_3 during the ASM. Finally, the model is used to determine the impact of regional pollution uplift, LiNOx and STE upon the CO and O_3 concentrations within this upper level AMA in section 5 and section 6 provides a summary and conclusions.

2 Observations and model

2.1 IASI O_3 and CO observations

The IASI instrument has been developed to fly on board the MetOp polar-orbiting platforms. The first 2 platforms, MetOp-A and B, were successfully launched in 2006 and 2012 respectively. IASI is a nadir viewing Fourier transform spectrometer observing the Earth-atmosphere Thermal Infrared Radiation (TIR) in the 645-2760 cm^{-1} wavenumber region (see e.g. Clerbaux et al. (2009)) with a resolution of 0.5 cm^{-1} after apodization. IASI provides global Earth coverage twice a day, with an overpass time at $\sim$9.30 and $\sim$21.30 local time, and a pixel size on the ground of 12 km at nadir.

IASI's primary objective is the delivery of accurate meteorological products to help to improve operational weather predictions. The IASI sensor can also monitor the tropospheric content of atmospheric trace gases such as O_3 (Eremenko et al., 2008; Barret et al., 2011) and CO (George et al., 2009; De Wachter et al., 2012). In the present study, we use data provided by the Software for a Fast Retrieval of IASI Data (SOFRID) presented in Barret et al. (2011) for O_3 and in De Wachter et al. (2012) for CO. In their study, Barret et al. (2011) showed that IASI enabled the independent retrieval of O_3 in the lower-middle troposphere (surface-225 hPa) and in the UTLS (225-70 hPa) in the tropics. Moreover, comparisons of SOFRID-O_3 data with data from O_3 sondes have shown that the agreement is especially good for the UTLS column (225-70 hPa) with correlation coefficients of 0.8 (resp. 0.95) and biases of 17.5$\pm$20% (resp. 10$\pm$ 10%) in Dufour et al. (2012) (resp. Barret et al. (2011)). The ability of SOFRID-O_3 to capture O_3 daily variations in the tropical upper troposphere has also been demonstrated and validated against MOZAIC cruise data in Tocquer et al. (2015). The SOFRID CO data have been validated against MOZAIC data in De Wachter et al. (2012). SOFRID data are able to capture the seasonal variability of CO at mid-latitudes (Frankfurt) as well as at tropical latitudes (Windhoek) in the lower (resp. upper) troposphere with correlation coefficients of 0.85 (resp. 0.70). At Windhoek, in the lower (resp. upper) troposphere SOFRID-CO data are biased low

with 13±20% (resp. 4±12%) compared to MOZAIC data.

2.2 MOZAIC O_3 and CO observations

The MOZAIC program was set up to provide routine measurements of reactive gases on long distance commercial aircraft (Marenco et al., 1998). In 1994, five airliners were equipped with O_3 and relative humidity instruments, and a CO analyzer was successfully added in December 2001. MOZAIC aircraft operations have stopped at the end of 2014. However, since 2011, a new set of instruments is flying on commercial in-service aircraft in the frame of the IAGOS (In-service Aircraft for a Global Observing System) Research Infrastructure. IAGOS builds on the scientific and technological experience gained within the two predecessors programs : MOZAIC and CARIBIC (http://www.caribic-atmospheric.com). The MOZAIC and IAGOS data follow the same calibration and quality control procedures and are freely accessible for scientific use at http://www.iagos.fr. The MOZAIC and IAGOS data are freely accessible for scientific use at http://www.iagos.org. These measurements are carried out with a 30 (resp. 4) s response time corresponding to a resolution of about 7 (resp. 1) km at cruise altitude and a vertical resolution of about 300 (resp. 30) m during ascents and descents, with a reported precision of ±5 (resp. 1) ppbv for CO (Nedelec et al., 2003) (resp. for O_3 (Thouret et al., 1998)). For the present study, we used MOZAIC profiles measured at take-off and landing near Hyderabad (17.2°N, 78.3°E) in central India from May to October 2009. CO data were available for each month but for O_3, no data were produced in September and October following an instrument failure. For both gases, we could use from 10 to 16 profiles for each month with available data.

2.3 GEOS-Chem configuration

In order to compute the CO and O_3 budgets in the Asian upper troposphere, we use the GEOS-Chem (GC) global chemistry transport model (Bey et al., 2001) version 9-01-01 with a set-up similar to that described in Yamasoe et al. (2015). This model has been thoroughly evaluated over the tropics through comparisons with in situ and remote sensed measurements of O_3, CO, NO_2 and HNO_3 (e.g. Martin et al. (2002) ; Sauvage et al. (2007a) ; Yamasoe et al. (2015)). GC is driven off-line by the meteorological analyses from the Goddard Earth Observing System (GEOS-5) of the NASA Global Modeling and Assimilation Office (GMAO). Tropospheric chemistry includes both O_3-NOx-hydrocarbons and aerosols chemistry. Stratospheric O_3 chemistry is computed with the linearized Linoz stratospheric ozone scheme developed by McLinden et al. (2000). STE are diagnosed with tagged O_3 simulations including a stratospheric O_3 tracer. Convection is parameterized with the relaxed Arakawa-Schubert scheme (Moorthi and Suarez, 1992) in GEOS-5. Turbulent mixing in the planetary boundary layer is described in Wu et al. (2007). The simulations are performed on a reg-

ular 2°x2.5° horizontal grid and on 47 hybrid pressure-σ levels from the surface up to 0.01 hPa. Emissions from Biomass Burning (BB) come from the monthly Global Fire Emissions Database version 2 (GFED-v2) (van der Werf et al., 2010). The global anthropogenic emissions are taken from the EDGAR v.4.1 inventory which provides annual global emissions of greenhouse gases and ozone precursors on a 1° x1° horizontal grid, but typically overwritten by data from various regional inventories. For instance over Asia we use the detailed inventory from Streets et al. (2006). Regional emission inventories are also used over Europe (EMEP), Canada (CAC), Mexico (BRAVO) and North America (EPA/NEI99 with ICARTT modification). All anthropogenic inventories are scaled for the year 2005. Biogenic emissions are taken from MEGAN v2.1. Detailed information on these emission inventories can be found on http://acmg. seas.harvard.edu/geos/doc/archive/man.v9-01-01/index.html. NOx emissions from lightning are computed according to cloud top height parameterization (Price and Rind, 1994), rescaled with LIS-OTD climatology (Sauvage et al. (2007a) ; Murray et al. (2012)) and are estimated at almost 6 Tg(N)/year (Martin et al., 2007).

We have performed 11 simulations for the May to October (MJJASO) period of 2009 with a six month spin-up. The control run was performed with all the emission sources considered. In order to determine the relative importance of the different sources on the CO and O_3 Asian UTLS budgets, we have performed sensitivity runs with emissions alternatively switched off. For CO, the sensitivity simulations concern South (0-40°N,60-100°E), East (15-40°N, 100-125°E) and South-East °S-15°N, 100-150°E) Asian anthropogenic and African (20°S-20°N, 20°W-50°E) BB emissions. For O_3, we considered the impact of NOx surface emissions from the same sources as for CO, and of LiNOx emissions from the two monsoon regions, South-Asia (0-40°N, 60-100°E) and Africa (20°S-20°N, 20°W-50°E). In order to investigate the stratospheric contribution on the AMA tropospheric ozone budget (section 5.2), we use a tagged ozone tracer to follow the stratospheric ozone flux across the tropopause as used in Sauvage et al. (2007b) and described by Fiore et al. (2002). The tagged simulation submits ozone produced in different regions of the atmosphere to archived three-dimensional fields of production and loss frequencies, allowing tropospheric ozone to be deconstructed into components from stratosphere and troposphere. The results from the sensitivity simulations are described and analyzed in section 5.1 for the CO budget and in section 5.2 for the O_3 budget.

2.4 IASI and GEOS-Chem comparisons

In order to validate the CO and O_3 distributions simulated by the GC model, we use SOFRID CO and O_3 retrievals to have a regional view of these distributions. The comparisons are made for monthly averaged profiles on the $2^\circ \times 2.5^\circ$ GC grid. The GC profiles are first interpolated on the 43 vertical retrieval levels from SOFRID. IASI vertical profiles have a vertical resolution ($\sim$6-8 km) that is much lower than those modeled by GC (100 m to 1 km). In order to take these resolution differences

into account and make a sound comparison, we have to convolve the GC vertical interpolated profiles with IASI averaging kernels (AvK) according to the classical smoothing equation (e.g. Barret et al. (2005); De Wachter et al. (2012); Liu et al. (2009)):

$$\hat{\boldsymbol{x}}_{\mathrm{GC}} = \boldsymbol{x}_{\mathrm{a}} + \mathbf{A} \cdot (\boldsymbol{x}_{\mathrm{GC}} - \boldsymbol{x}_{\mathrm{a}}) \quad (1)$$

where $\boldsymbol{x}_{\mathrm{GC}}$ and $\hat{\boldsymbol{x}}_{\mathrm{GC}}$ are the original and the smoothed or convolved GC profiles. $\mathbf{A}$ is the SOFRID AvK matrix which describes the sensitivity of the retrieved to the true profile (see Rodgers (2000) for a description of the AvK matrix) and $\boldsymbol{x}_{\mathrm{a}}$ is the a priori profile used for the retrieval (the description of the a priori profiles can be found in Barret et al. (2011) for O_3 and De Wachter et al. (2012) for CO).

3 Modeled versus observed CO and O_3 distributions

The comparisons of the tropospheric CO/O_3 Asian distributions simulated by GC and observed by IASI enable us to evaluate the model's capacity to reproduce the large scale features of the distributions and the possible causes of discrepancies. Airborne MOZAIC profiles measured in central India will provide a more precise evaluation of the absolute values simulated locally by the model.

3.1 CO in the Asian troposphere

The monthly distributions of UTLS (270-110 hPa) CO columns from IASI and GC are displayed in Fig. 1 for the region extending from Africa to Indonesia and from 10S° to 40°N for the May (pre-monsoon) to October (post-monsoon) period. The dominant features of these distributions are the maxima over Africa and Asia. The statistics of the CO UTLS columns comparison (for the domain displayed in Fig. 1 and the 6 months from May to October) are summarized in Table 1. GC understimates the columns by 11$\pm$9% relative to IASI with a correlation coefficient of 0.70. The smoothing has little impact on the bias but reduces the relative standard deviations of the differences and enhances the correlations. The comparison between GC simulations forced with GEOS-5 analyses and MLS at 215 hPa for the tropical band of Liu et al. (2013) gives similar results with a 10 ppbv bias and a correlation coefficient of 0.65.

Over Africa the observed maximum shifts from western Africa in May to Central and Southern Africa in July and September following the BB season (Sauvage et al., 2005) . We notice that the GC upper tropospheric CO distributions over Africa display the same kind of discrepancies with IASI

than those shown by Liu et al. (2010, 2013) with MLS. Indeed, their GC simulations have CO concentrations that are systematically too low at 215 hPa over Central Africa in July (Liu et al., 2013) and from August to October (Liu et al., 2010). Furthermore, Barret et al. (2010) have shown that 5 CTMs using GFEDv2 for BB emissions underestimate the upper tropospheric CO concentrations during the monsoon over Africa between 10°S and 5°N by up to 50 ppbv compared to MOZAIC in-situ data. The use of the BB emission inventory from Liousse et al. (2010) leads to a correction of these biases and even to an overestimation of modeled upper tropospheric CO over Africa. The bias documented here probably results from too low BB emissions over central and southern Africa from GFEDv2. Nevertheless, African BB emissions are not expected to impact the AMA composition and the observed biases will not impact our results.

Over Asia, which is the focus of our study, the highest CO columns are simulated by GC and detected by IASI over East Asia before the monsoon (May), over the continental convective region corresponding to Northern India, Nepal and southern Tibet during the monsoon (JJA) and back over East Asia after the monsoon (September-October). We have used a threshold of 2.5 kg/m^2/s for the upward convective mass flux from the GEOS-5 analyses in the upper troposphere (350-150 hPa) to identify the deep convective areas (see contours in Figure 1). The ASM region is indeed characterized by GEOS-5 upward convective mass flux values comprised between 1 and 5 kg/m^2/s in the upper troposphere (not shown) and 2.5 kg/m^2/s corresponds to relatively strong convective uplift. During July and August, high CO UTLS columns are also captured by the model and IASI within the AMA, as has already been documented in Park et al. (2009) and Barret et al. (2008). The AMA is delimited by the 12520 m GH contour at the 200 hPa level, as done in Randel and Park (2006) (see section 4.1 for the definition of the AMA boundaries). More specifically, IASI detects enhanced CO columns in agreement with raw GC columns over the monsoon region and underestimates the CO columns in the western part of the AMA. This is an effect of IASI's limited vertical sensitivity, as appears from the GC UTLS distributions once the profiles are smoothed by IASI averaging kernels according to equation 2.4 (Fig. 1 second column) resulting in lower UTLS columns and a better agreement with IASI. This is confirmed by the longitude-pressure cross-sections averaged over the 21-29°N band that correspond to the southern part of the AMA (Fig. 2), where we notice that the AvK smoothing mixes the UTLS enhanced concentrations throughout the middle and upper troposphere, leading to a better agreement with IASI cross-sections. In the eastern part of the AMA, CO UTLS concentrations are higher and better detected by IASI, resulting in a lesser effect of the smoothing and a better agreement between IASI and GC raw columns. Our results apparently disagree with Liu et al. (2013), who report larger underestimations of UTLS GC CO over Asia than elsewhere in July 2005 especially at 100 hPa. They argue that this model underestimation probably results from insufficient convective uplift to 100 hPa with GEOS-5. Indeed, our comparisons with IASI (Fig. 1) do not show enhanced underestimation of the GC UTLS columns in the Asian region and in the AMA. The low

vertical resolution of IASI and its lack of sensitivity above 150 hPa highlighted in Fig. 2 are probably responsible for this apparent contradiction with Liu et al. (2013).

The good agreement of IASI and GC in the middle and upper troposphere within the enhanced CO region is confirmed by looking at the latitude-pressure cross-sections averaged over the 75-105°E longitude domain where convection is active (Fig. 3). IASI clearly detects the UTLS enhanced CO concentrations between 400 and 200 hPa resulting from convective detrainment in very good agreement with GC. Kar et al. (2004) have already shown that the MOPITT sensor was able to detect UTLS CO enhancements disconnected from the lower troposphere and resulting from convective detrainment during the ASM. Our IASI latitude-pressure cross sections clearly show that IASI is also able to detect such CO UTLS bubbles. Both IASI and GC document that the southern edge of the CO enhancements shifts from 10 to 20°N from May to July and back to 10°N from August to October (Fig. 3). Nevertheless, GC underestimates CO throughout the troposphere around 15°N particularly in May-June. These results are confirmed by CO profiles measured by the MOZAIC programme in Hyderabad (Fig. 4). In the middle and upper troposphere, the agreement between MOZAIC and GC is within the 1σ variability, except during the May-June period, characterized by an important CO underestimation by GC, with however good modeling of the CO seasonal variation. Finally, enhanced UTLS CO columns from August to October over Indonesia also correspond with CO enhanced concentrations between 500 and 200 hPa at the Equator in both IASI and GC distributions in Fig. 3.

Even if the focus of our study is the upper troposphere, we note that during the May-October period, high CO concentrations are detected by IASI and simulated by GC in the lower and middle troposphere within the monsoon polluted region over 20-35°N (Fig. 3) and 70-120°E (Fig. 2). Enhanced CO concentrations ($>$ 110 ppbv) are also detected by IASI west of 70°E over the Middle East and northern Africa (Fig. 2) where the model simulates lower CO concentrations even if the model-satellite bias is partly corrected when smoothing by the AvK is taken into account. The smoothing is responsible for mixing high CO concentrations simulated close to the surface to the lower and free troposphere. The discrepancy between GC and IASI in the free troposphere is larger between May and August than in September-October. The study of Liu et al. (2010) also documents an underestimation by GC of TES for CO at 681 hPa over the Middle-East and northern Africa that is larger in August than in September and October 2005 (see their Figure 3). The underestimation of CO by the GC in the lower and middle troposphere also appears south of 20°N in Fig. 3. Comparisons between GC and MOZAIC profiles in Hyderabad (Fig. 4) confirm these overly low CO concentrations simulated by GC below 600 hPa with decreasing differences from June to October.

Concerning the upper troposphere, both GC and IASI are able to capture the seasonal variability associated with the ASM and particularly the CO enhancements within the AMA. It is noteworthy that IASI enables the detection of uplifted CO in the ASM region. Nevertheless, GC significantly underestimates CO in the lower and middle troposphere during boreal spring over India compared with IASI and MOZAIC.

3.2 O_3 in the Asian troposphere

Concerning O_3 GC versus IASI comparisons, it is important to note that using equation 2.4 to smooth GC profiles implies mixing stratospheric O_3 concentrations in the UTLS column. The averaging kernels displayed in Barret et al. (2011) show for instance that the O_3 concentration retrieved at 150 hPa is sensitive to O_3 up to about 50 hPa. Stratospheric biases in the model would therefore imply an apparent bias in the modeled UTLS column compared with IASI. As mentioned above, we use GC version 9-01-01 which stratospheric O_3 is based on the linearized scheme from McLinden et al. (2000). Recently Eastham et al. (2014) have evaluated stratospheric O_3 from GC version 9 (using Linoz) versus a new version (not publicly available at the time of this study) using the Universal tropospheric-stratospheric Chemistry eXtension (UCX). They show that, averaged annually, GC-Linoz total columns of ozone are biased by 25 to 50 DU compared with TOMS in the band from 40°S to 40°N. The annual averaging hides much larger regional and seasonal discrepancies. Indeed, from their Fig. 2 we can roughly estimate that for the May-October period of interest here, the overestimation of the total columns can reach 100 DU in the tropics and in the southern hemisphere, down to 60°S. From Dufour et al. (2012), we also know that SOFRID stratospheric O_3 is highly biased compared to ozonesondes with biases of $8\pm5\%$ for the column up to 30 km and $7\pm5\%$ for the stratospheric (16-30 km) column. Comparisons between IASI and GC for the May-October period in the 30°S-30°N band show that the mean GC stratospheric (90-24 hPa) column is 1.66 times higher than IASI mean column. Taking the 7% IASI bias in the tropics into account, we have applied a 0.58 scaling factor to GC profiles in the lower and middle stratosphere (90-24 hPa) before applying the AvK smoothing.

The UTLS O_3 columns are displayed in Fig. 5. The most obvious feature of the distributions captured by IASI and GC is the transition from low columns in the tropical UT south of the tropopause (2PVU) to high columns in the extra-tropical lower stratosphere. This transition closely follows the undulation of the tropopause. From June to September, the tropopause is pushed northwards by the AMA circulation and the region from the Middle East to East Asia is characterized by intermediate O_3 columns. The region of lowest O_3 columns is simulated and observed over the western Pacific in May and progresses northwestwards to South-East Asia and South India until October. Over Africa, IASI and GC document a southward shift of moderate O_3 columns from western Africa in May

345 to southern Africa in September-October. This general good agreement between IASI and GC O_3 distributions translates into correlation coefficients higher than 0.9 and a mean bias of 14±26% (see Table **??**). Biases between IASI-SOFRID and UTLS columns from ozonesondes were estimated to be 17.5±19.3% (Dufour et al., 2012) and 10±10% (Barret et al., 2011) once the ozonesondes profiles were smoothed by IASI AvK. The mean value of the GC UTLS columns over our study region
350 is therefore most likely to be in good agreement with ozonesondes. The good behavior of GC UTLS O_3 is corroborated by comparisons between GC and MOZAIC profiles at Hyderabad which show a very good agreement between the surface and 200 hPa during the May-August period (see Fig. 4). Unfortunately, no O_3 data are available from MOZAIC Hyderabad-Frankfurt flights in September and October 2009.

355

When smoothing is applied to GC profiles, the features of the O_3 distribution remain similar but some corrections are introduced. Over most of the domain, the GC UTLS columns are slightly increased leading to a better agreement with IASI with differences within ± 50%. On the other hand, over the oceanic convective regions of the western Pacific characterized by the lowest O_3 absolute
360 values, the smoothing tends to decrease the UTLS column leading to the highest relative biases (exceeding -50%). This decrease of UTLS O_3 when IASI AvK are applied has already been reported in Dufour et al. (2012) for ozonesonde profiles as a result of the accentuation of the O_3 S-shape for tropical profiles. The effect is therefore more important for convective oceanic profiles which have the most marked S-Shape.

365

The latitude-pressure cross sections displayed in Fig. 6 highlights the impact of the convolution of the modeled profiles by IASI AvK to smooth the lower stratosphere to upper troposphere transition and to decrease the height of the chemical tropopause. The very low O_3 concentrations from the model smoothed profiles over the Bay of Bengal convective region (south of 20°S) result from the
370 accentuation of the S-shape profiles discussed above. These cross-sections also indicate the northwards shift of the tropopause and of high UTLS (300-150 hPa) O_3 concentrations from May until September. It is interesting to note the large O_3 concentrations originating from the stratosphere in the middle troposphere down to 700 hPa between 20 and 30°N in May and June that almost disappear in July and August, only to reappear in October. The seasonal variations of STE that both
375 model and observations are pointing to are in good agreement with the results from Cristofanelli et al. (2010) which, based on in-situ data in the Himalaya, indicate the absence of stratospheric intrusions during the monsoon season.

Fig. 7 presents the O_3 longitude-pressure transects over Asia. In the middle-upper troposphere,
380 both model and observations display a persistent west-east gradient with lower O_3 concentrations east of 70°E. This gradient is the highest during the Asian monsoon period when convection is the

most active in the western part of the domain and when the Middle-East is characterized by its annual O_3 maximum (Li et al. (2001); Liu et al. (2009, 2013)). Nevertheless, from June to September, the UT O_3 concentrations are not homogeneously low in the convective region and enhanced O_3 concentrations are simulated and observed between 100 and 120°E. In the model, the lowest UT O_3 concentrations coincide with the deepest convection centered around 75°E, and the enhanced concentrations coincide with less intense convection, as illustrated by the 2.5 kg/m^2/s convective upward mass-flux contour.

The general features of the tropospheric and UTLS O_3 distribution over the large Asian region simulated by the GC are in good agreement with those observed by IASI. The application of the AvK convolution to GC vertical profiles decreases the altitude of the chemical tropopause, smoothes some of the modeled high resolution features and accentuates the S-shape of convective oceanic O_3 profiles. Nevertheless, the model and IASI display the same longitudinal and latitudinal gradients, both in the middle and in the upper troposphere over Asia.

4 Dynamical and chemical characterization of the AMA

The first part of this section is dedicated to the characterization of the AMA as a 3D volume based on dynamical parameters to enable the quantification of chemical budgets within this upper level anticyclone (section 5). We will then discuss the dominant role played by convection in controlling tropospheric CO and O_3 distributions over Asia and more particularly within the AMA.

4.1 The Asian Monsoon Anticyclone: a 3D volume

During May and October, the convective activity mostly takes place over southeast Asia and the 150 hPa tropopause is located between 30 and 35°N over Asia and the AMA is not present (see Fig. 1). In June and September, at the beginning and at the end of the ASM, the convective activity has moved northwards towards the Bay of Bengal and the AMA is present over northeastern South-Asia. During the heart of the ASM (July-August), the region impacted by convection encompasses the Bay of Bengal, India, Bangladesh, Nepal and southeastern Tibet and the tropopause is pushed to 40° north by the AMA which is fully developed and extends roughly from 20 to 40°N and from 30 to 120°E and vertically from 300 to 100 hPa. The center of the AMA is bimodal with the high pressure center located alternatively over the Tibetan plateau and over Iran (Zhang et al., 2002). This high level anticyclone is characterized by large scale periodic elongations and sheddings as described in Popovic and Plumb (2001). The AMA air masses are characterized by low potential vorticity (PV) values or high geopotential heights (GH). **Based on MLS CO analyses Barret et al. (2008) have shown that daily CO and PV variations were strongly correlated with low PV related to high CO. In the Asian UTLS, the tracer concentration is therefore strongly controlled by the oscillations**

and sheddings of the AMA. In their study about the AMA strength and variability, Garny and Randel (2013) have also pointed to the spatio-temporal correlation of CO enhancements and low PV values which is stronger in the upper levels of the AMA. Based on PV fields Ploeger et al. (2015) have developped a method to characterize the dynamical barrier that delimit the inside and the outside of the AMA on a daily timescale. The boundaries of the AMA based on their method are consistent with tracer concentrations (high CO and low O_3 within the AMA). In studies looking at monthly or seasonal timescales, the edge of the AMA has been mostly defined as simple constant GH contours at different pressure levels. Randel and Park (2006) (resp. Heath and Fuelberg (2014)) use a 14320 (resp. 14430) m GH for the AMA at 150 hPa and Bergman et al. (2013) use 12520 (resp. 16770) m GH at 200 (resp. 100) hPa.

In order to determine the CO and O_3 budget within the AMA, we first need to characterize the AMA as a closed volume and we have therefore looked for a criterion independent of the pressure level. As already discussed, the studies based on PV (Barret et al., 2008; Garny and Randel, 2013; Ploeger et al., 2015) have shown that it was a good dynamical parameter to charactrize the AMA high frequency variability whilst GH was mostly used on monthly timescales (Randel and Park, 2006; Bergman et al., 2013; Heath and Fuelberg, 2014). Furthermore, Ploeger et al. (2015) is the only study that proposes a PV-based criterion to delimit the AMA but this criterion is only defined and validated for the 380 K potential temperature level ($\sim$ 200hPa). As the PV tracer relationship is stronger at the higher levels (380K) of the AMA (Garny and Randel, 2013) the criterion from Ploeger et al. (2015) may not hold for the lower levels. Finally, on monthly timescales, simple GH thresholds have been shown to consistently delimit regions of tracer anomalies characteristic of the AMA at different pressure levels. We have therefore chosen to use a criterion based on GH rather than PV to delimit the AMA. Our criterion is based on thresholds of GH anomalies. We use the GH **monthly** fields from the MERRA re-analyses which are provided on 42 levels from the surface to 0.1 hPa with a 1.25°X1.25 ° horizontal resolution. The anomalies are computed as the differences between the mean zonal GH computed over the 50°N to 50°S latitudinal band and the local GH. The AMA appears very clearly at different UTLS levels as the region with the highest GH anomalies on Fig. 8. The contours corresponding to a 270 m GH anomaly best match the 16770, 14320 and 12520 m GH isocontours at 100, 150 and 200 hPa corresponding to the AMA edge in Bergman et al. (2013), Randel and Park (2006) and Bergman et al. (2013) respectively. We have therefore chosen a 270 m GH anomaly as the threshold for the AMA boundary throughout the UTLS. In section 5, within the AMA and outside of the AMA both refer to the tropospheric part of these atmospheric regions bounded by the 2PVU contour.

4.2 Relationship between convection and the CO and O_3 distributions

The studies presented in the introduction have highlighted the AMA as a region with a composition that is very different from its surroundings, according to UTLS satellite observations. The use of IASI data brings information about CO and O_3 over the whole troposphere and therefore allows to better document the link between the upper tropospheric distributions and transport processes such as convection. In the following paragraph, we analyze the modeled and observed O_3 and CO distributions in light of their relationship with convection.

In the middle troposphere, the longitude-pressure sections of CO and O_3 presented above are anti-correlated. East of about 80°E, in the monsoon region characterized by the strongest convective upward mass fluxes from GEOS-5, high CO (90 ppbv) is associated with low O_3 (60 ppbv) and West of 80° E low CO is associated with high O_3. This anti-correlation is clear both from the model outputs and from IASI data. The high summer tropospheric O_3 extending from western India to north Africa has been first described as the "Middle East tropospheric Ozone maximum"by Li et al. (2001) and further analyzed by Liu et al. (2009, 2010). The subsidence associated with the AMA is taking place in the middle troposphere on its western side over the Eastern Mediterranean, the Middle East and Central Asia (Hoskins and Rodwell, 1995; Liu et al., 2009). This phenomenon is clearly seen in Fig. 9 that displays GC O_3 fluxes in a longitude pressure cross-section at the center of the AMA. This descent of air masses impacted by Asian pollution trapped within the AMA contributes to the summer "Middle East tropospheric Ozone maximum". In their analysis, Liu et al. (2009) have shown that the O_3 buildup is favored by the Arabian and Saharan anticyclones that isolate the middle troposphere over this region. From simulations with tagged O_3 Liu et al. (2009, 2010) attribute an equivalent and dominant impact (30-35%) on the O_3 maximum over the middle East to local sources and transport from Asia via the UT and the AMA circulation. Over Northern Africa, transport from Asia contributes less thann regional sources. It is clear from the CO GC distributions displayed by Liu et al. (2009) (their Fig. 6) and from the present study as well as from our IASI data (Fig. 2 and 7) that the O_3 Middle East maximum in the middle troposphere coincides with relatively low CO concentrations.

Between 80 and 120°E, the low O_3 and high CO concentrations result from the convective activity occurring in South and South-East Asia during the monsoon. Convection mixes CO between the Asian polluted PBL and the upper troposphere resulting in enhanced concentrations over the whole troposphere. The overlap between important CO sources and convection occurs primarily over the Indo-Gangetic Plain (IGP) according to Fig. 10 that displays anthropogenic CO emissions from the Streets inventory (Streets et al., 2006) and GEOS-5 upward convective mass fluxes. The impact of convective transport on the O_3 distribution is more complicated. It results from two antagonist effects: the vertical mixing of O_3 itself and the uplift of O_3 precursors followed by enhanced photochemical O_3 production (Doherty et al., 2005; Lawrence et al., 2003). The vertical mixing results

in the transport of O_3 poor air masses from the lower troposphere where O_3 lifetime is short to the upper troposphere where it is long and O_3 rich air masses from the upper to the lower troposphere by compensatory subsidence. The effect of this overturning is a decrease of UT O_3 and of the tropospheric O_3 burden and lifetime. Over polluted regions, such as Asia, convection uplifts O_3 precursors (especially NOx) result in an increase of the O_3 production in the middle and upper troposphere at the expense of the lower troposphere. The electric activity from convective storms is responsible for the in-situ production of LiNOx, also responsible for an increased O_3 production. This source of O_3 clearly appears in Fig. 9 where the net O_3 production rates are enhanced between 500 and 150 hPa in the monsoon region. Convective clouds also diminish the tropospheric photochemical activity through a reduction of the solar UV radiations. These combined effects are responsible for the lower **mid-tropospheric** O_3 concentrations over South Asia compared to regions with high insolation and downward transport of O_3, such as the Middle East and North Africa.

In the Asian upper troposphere in June, the AMA is building up and only extending between 60 and 120°E and the O_3 fluxes switch from downward to upward around 90°E (Fig. 9). In July and August, the AMA is well established over the 15-145°E domain and the upward flux remains east of 90°E in the monsoon region while the strongest downward fluxes move to the western edge of the AMA between 15 and 45°E. As already discussed, this downward flux **partly** contributes to the build-up of the Middle East O_3 maximum as described in Liu et al. (2009). In September, the situation is similar to June, the AMA has largely shrunk and the O_3 production is associated with an O_3 downward flux between 75 and 90°E. Above the continents, the photochemistry illustrated by the O_3 net production rates in Fig. 9 switches from a net source of O_3 in the polluted PBL, to a net sink in the free troposphere below about 500 hPa and again to a net production in the middle and upper troposphere. This behavior agrees with the different NOx photochemical regimes discussed in Jacob et al. (1996). In particular, low NOx concentrations are responsible for the destruction of O_3 in the lower and middle troposphere and slightly higher concentrations produce O_3 in the upper troposphere, as explained in (Brune, 1992, IGAC Report). During the whole period, the O_3 net production pattern in the middle and upper troposphere is characterized by a double maximum with values exceeding 5 ppbv/day that are associated with the upward fluxes east of 90°E and downward fluxes (except in August) west of 90°E. Both upper troposphere maxima are located within the eastern half of the AMA. Below the tropopause, the O_3 net production rate is exceeding 2 ppbv/day within the whole AMA. The enhanced net O_3 production rates are associated with enhanced NOx concentrations (100 pptv contour in white). In the upper troposphere, the AMA therefore appears as a region of high O_3 production, resulting from the trapping of NOx from various sources. In the next section, we determine the impact of the different sources on the CO and O_3 budgets within the AMA.

5 CO and O_3 budget

Our aim here is to characterize the origin of CO and O_3 within the Asian upper troposphere during the monsoon season by comparing the impact of the different emission sources inside and outside of the AMA based on sensitivity simulations for the different type of emissions and for the different regions of interest. For CO we have considered anthropogenic and BB emissions and for O_3 we have considered the production of NOx originating from anthropogenic, BB and lightning sources and the transport of stratospheric O_3 through STE.

5.1 The CO budget

As mentioned in section 2.3, we have considered the two main regions of importance concerning anthropogenic CO emissions: South and East Asia. Park et al. (2009); Yan and Bian (2015) have indeed highlighted the predominant role of Asian sources from these two regions in filling the AMA with CO. We can also notice that the surface fluxes of CO used for our GC simulations (Fig. 10) are the largest for the whole Asian region over north-eastern China and for the South-Asian domain over the IGP. These fluxes are consistent with those used in Park et al. (2009) and Yan and Bian (2015). Concerning BB, Nassar et al. (2009) have shown that Indonesian BB emissions had a large impact on the Indian upper troposphere composition in 2006 following the perturbation of the tropical circulation by a strong El Nino event. Our sensitivity simulations performed for Indonesian or South East Asian anthropogenic sources have shown that in 2009 this region was not impacting the south Asian upper troposphere (not shown). The simulation with African BB CO emissions switched off also results in negligible modifications of the CO distribution in the south-Asian upper troposphere (not shown).

The differences between the reference simulation and the sensitivity simulations with anthropogenic CO emissions from South and East Asia shut down are displayed in Fig. 11 for the pressure-longitude section (21-29°N) and in Fig. 12 for the upper tropospheric (200 hPa) distribution. The average CO mixing ratio differences between on and off simulations within and outside of the AMA are given in Table 2. The pressure-longitude sections clearly show that the upper troposphere and especially the AMA ones are more impacted by South Asian than East Asian emissions. For the 4 months considered, CO from South Asia is responsible for CO enhancements of 20 to 30 ppbv within the AMA between 300 and 100 hPa, while East Asian emissions mostly impact regions below 200 hPa on the eastern side of the AMA. This result is expected from the correlation between high emissions and strong convection over South Asia as can be seen in Fig. **??**. High convective mass fluxes (> 2.5 kg/m^2/s) at 225 hPa are located over the IGP, where CO emission fluxes exceed 150 kg/km^2/day. East of the Himalaya, the emissions are largest over eastern China where convection is not as strong as over the IGP. The region with the strongest South-Asian CO uplift in the

middle troposphere lies between 75 and 105°E according to the GC (see Fig. 11) which is consistent with Bergman et al. (2013), who highlights that PBL air masses that reach the UTLS pass through a mid-tropospheric conduit located roughly over the same region.

In the upper troposphere at 200 hPa, East Asian emissions are only responsible for CO enhancements of about 10-20 ppbv located over south-east Asia and China during the monsoon. Larger CO enhancements are caused by South Asian emissions with the highest values ($>$ 35 ppbv) located within the convective region around 75°E and 27°N and values exceeding 20 ppbv that spread within the AMA bounded by the tropopause to the north. These values are higher than those of Yan and Bian (2015), who found CO enhancements of 12-30 ppbv from Indian sources and of 5-9 ppbv from Chinese sources at 215 hPa. At 100 hPa (not shown), East Asian sources contribute to less than 6 ppbv to UTLS CO which is slightly lower than what Yan and Bian (2015) and Park et al. (2009) have documented. Concerning South Asian sources, they are responsible for 12 to 20 ppbv CO enhancements (not shown) in good agreement with Yan and Bian (2015) and Park et al. (2009). **Vogel et al. (2015) have also quantified the origin of PBL air masses in the AMA using artificial emission tracers from the CLaMS CTM. Their emission regions are different from those used in the present study. India is separated in Northern and Southern India and South East Asia encompasses our South East Asia and part of our East Asia (most of the Indochinese peninsula). Nevertheless, their results show some agreement with ours and give some complementary information. They show that when the AMA is established, BL airmasses coming from Northern India are filling up the AMA comparably to our South Asian tracer which indicates that Southern India plays a minor role. Their South East Asian emission tracer is transported upwards and remains at the edge of the AMA such as our East Asian tracer (especially for August which is not shown). The agreement probably comes from the fact that both tracers encompasses the Indochinese peninsula where convection is strong during the monsoon but which is located to the south of the AMA.**

The average figures of Table 2 summarize these results. South Asian CO emissions are responsible for a strong CO enhancement within the AMA from June to September with a maximum of $\sim$25 ppbv during the monsoon peak in July-August. Furthermore, average CO enhancements from South Asian emissions are about 10 ppbv larger within than outside of the AMA which further highlights the AMA as a trap for uplifted South-Asian pollution during the monsoon. East-Asian emissions result in maximum enhancements of about 10 ppbv in the UTLS during July-August. The little differences between the enhancements computed within and outside of the AMA also show that East-Asian sources are located outside of the conduit connecting boundary layer air masses and the AMA described in Bergman et al. (2013).

5.2 The O_3 budget

The contribution to the O_3 burden from the main sources of NOx emissions is computed from sensitivity simulations with the GC model. Sauvage et al. (2007b) have shown that tropospheric O_3 over Asia during the monsoon is mostly impacted by Asian sources. Focusing on the Indian region, Kunhikrishnan et al. (2006) have also highlighted the predominance of Asian sources (India, China and Indonesia) on the Indian tropospheric O_3 budget during the monsoon. They have also shown that Middle-East emissions have a small impact on NOx and O_3 concentrations below 500 hPa and that African and Middle-East sources have a negligible impact in the middle and upper troposphere over India during the ASM. We have therefore chosen to focus on the impact of Asian emissions upon the AMA O_3 burden. Concerning anthropogenic emissions, we have separated Asia into the same three main regions as for CO (see section 2.3). One of the main conclusion of Sauvage et al. (2007b) is that LiNOx is the most important NOx source controlling the tropical tropospheric O_3 burden. We therefore performed simulations to characterize the importance of LiNOx from the two nearby monsoon regions (see 2.3) upon upper tropospheric O_3 during the ASM. Finally, the impact of STE was established using the GC stratospheric O_3 tagged tracer as explained in section 2.3.

For O_3, the results of the sensitivity simulations are displayed in Fig. 13 for longitude-pressure sections averaged over the 21-29°N band and in Fig. 14 for maps at 200 hPa. The results are summarized in Table 3 for O_3 and NOx average mixing ratios. The enhancements of O_3 by NOx anthropogenic emissions from South and East Asia are closely linked to those of CO previously analyzed. As for CO, sensitivity simulations with Indonesian anthropogenic and African BB NOx sources switched off (not shown) show very little impact on South Asian upper tropospheric O_3.

The O_3 enhancements caused by East-Asian emissions is the largest ($>$ 15 ppbv) below 300 hPa between 90 and 120°E. Convection is not strong enough over China to bring PBL NOx deep into the AMA and on average, upper tropospheric O_3 enhancements from Chinese emissions are about 5 ppbv both within and outside of the AMA during July-August. Compared to Chinese emissions, South-Asian emissions have a smaller impact on free tropospheric O_3 ($<$12 ppbv) but a larger scale impact on O_3 in the upper troposphere and more specifically within the AMA. On average, South-Asian emissions are responsible for an O_3 (resp. NOx) increase of 8 (resp. 0.04) ppbv within the AMA and of about 5 (resp. 0.015) ppbv outside of the upper-level anticyclone (Table 3). Indian NOx are uplifted and trapped within the AMA (see white contours in Fig. 14) and produce O_3 molecules that are also trapped within the AMA.

Asian LiNOx are responsible for an important O_3 production in the Asian upper troposphere mostly confined within the AMA (see Fig. 13 (h) and (m)) with a strong intra-seasonal variability. In July, LiNOx produce 13.5 ppbv O_3 in the AMA and only 10 ppbv in August. In both cases, the O_3

production outside of the AMA is half of its value within the AMA. For NOx, the production within the AMA is about 2.5 higher than outside of the AMA, highlighting the non-linearity of the O_3 production by NOx. The impact of African LiNOx over Asia varies strongly from June to September. In June and September, when the AMA is weakened and located east of 90°E, African LiNOx have a large impact in the upper troposphere over the Middle-East and in the free troposphere further east over India (Fig. 14). In July and August, the AMA circulation that extends to 30°W prevents air masses impacted by African LiNOx from affecting O_3 in the Middle-East upper troposphere and the free troposphere over India is also less impacted than in June and September. During the July-August period, the large subsidence over the Middle-East (30-60°E) (see Fig. 9 (b) and (c)) brings O_3 produced by both South Asian anthropogenic NOx and Asian LiNOx down to **400 hPa** (Fig. 13 (g) and (h)) and contributes to the **upper part of the** mid-tropospheric O_3 maximum. **Below 400 hPa and down to 600 hPa, the air masses coming from the West are not blocked by the AMA and both African LiNOx and STE have a larger contribution to the free tropospheric Middle-East O_3 maximum (Fig. 13 (i) and (j)) highlighted by GC and IASI (Fig. 7 (d) and (f)) than Asian sources**.

The last source of O_3 in the Asian upper troposphere that we investigated is STE. At 200 hPa, STE is not an important contributor to the O_3 distribution, as can be seen in Fig. 14. At this pressure level, stratospheric O_3 rich air-masses are kept outside of the AMA circulation. Nevertheless, on average, STE contributes from 7 to 12 ppbv O_3 within the AMA (Table 3). These high values are caused by STE impacting the upper troposphere between 150 hPa and the tropopause, as highlighted by the stratospheric O_3 tracer cross-sections in Fig. 13. It is also interesting to note that STE also impacts the free troposphere over the Middle-East and India in a very similar way to African LiNOx, traveling with the westerly winds below the AMA. The same eastward transport of Middle-East NOx emissions has been shown to slightly ($\sim$10%) impact NOx and O_3 distributions in the lower troposphere over India (Kunhikrishnan et al., 2006). Nevertheless, as discussed in Section 3, O_3 from GEOS-Chem is overestimated in the lower and middle stratosphere (24-90 hPa) by a factor of $\sim$1.7. This overestimation most likely implies a similar overestimation in STE evaluated with the O_3 stratospheric tracer and STE is probably responsible for a 4 to 7 ppbv O_3 enhancement in the AMA.

Asian LiNOx therefore appear to be the largest NOx source within the AMA with a contribution to the NOx concentration that is twice to three times larger than South-Asian anthropogenic NOx emissions. This result appears contradictory to that of Kunhikrishnan et al. (2004) who estimated that during the monsoon in the Indian upper troposphere, 60 to 70 % of NOx come from local surface sources and only 20-25% from LiNOx. This apparent contradiction is due to the fact that Kunhikrishnan et al. (2004) defines the upper troposphere as the 500-150 hPa while the AMA spans the 300-100

hPa domain and, according to Fig. 13, LiNOx have their largest impact between 200 and 100 hPa. Furthermore, the global annual LiNOx source used in Kunhikrishnan et al. (2004) is 2.8 Tg(N)/year which is in the lower part of the 6±3 Tg(N)/year estimation from Schumann and Huntrieser (2007). In our GEOS-Chem simulations, the global annual LiNOx source is set to 6 Tg(N)/year. Concerning the impact of NOx local sources on the upper tropospheric (500-150 hPa) O_3, Kunhikrishnan et al. (2004) found a maximum of 15%. Similar results are found by Kunhikrishnan et al. (2006) with a 10 to 20% sensitivity of O_3 to Indian NOx emissions in the middle and upper troposphere (700-200 hPa) over India. From Fig. 14 (g) and (l), we can roughly estimate a production of 9 ppbv in the 500-150 hPa range and 60-95°E by Indian NOx sources. For the same region, we also estimate a rough average of 60 ppbv O_3 for the July-August period from Fig. 7 (g) and (j). We have therefore an approximate 15% sensitivity of O_3 to the Indian NOx source in good agreement with Kunhikrishnan et al. (2004, 2006). According to Kunhikrishnan et al. (2006), NOx emissions from Indonesia have a non-negligible effect on upper tropospheric NOx (20-30%) and O_3 (10-15%) over India during the ASM period. They also state that the impact of Indonesian emissions is more important over the southern part of India through transport by the tropical easterly jet, which was especially strong in the 1997 El-Nino year. This does not contradict the negligible impact of Indonesian emissions on the AMA composition that we have reported, the AMA being an isolated region north of the tropical easterly jet.

6 Summary and conclusions

In the present study, we have analyzed the CO and O_3 distributions and budget in the upper level AMA based on observations from the Metop-A/IASI sensor and on simulations from the global chemistry transport model GEOS-Chem. Model simulations and spaceborne observations have shown a good general agreement for regional features and the seasonal variations of the upper troposphere distributions, with correlation coefficients of 0.70 for CO and 0.94 for O_3. The higher correlation for O_3 results from its high variability between the oceanic tropical upper troposphere and the extra-tropical lower stratosphere. Low CO bias in the lower-middle troposphere has been diagnosed in the simulations with both spaceborne IASI and MOZAIC in-situ data. Such a bias was already identified by other studies with GC (Liu et al., 2010, 2013). The convective uplift of CO is clearly detected by IASI in the monsoon region but the enhanced upper tropospheric CO resulting from westward transport in the AMA circulation is smoothed over the middle and upper troposphere. For O_3, large biases resulting from an accentuation of the S-shape profiles by the AvK smoothing are found over the tropical oceanic regions.

Based on our IASI observations and model simulations, we have analyzed the CO and O_3 distributions in relation with the AMA and monsoon convection. We first developed a method to characterize the 3D boundaries of the AMA based on geopotential height (GH). We found that the AMA could be defined as the region with GH differences larger than 270 m relative to the GH averaged over the 50°S to 50°N band. Both observations and simulations have revealed an anti-correlation of O_3 and CO in the middle and upper troposphere, with lower (resp. higher) O_3 (resp. CO) in the eastern part of the domain corresponding to the ASM region than in the western part over the Middle-East, North Africa and the Eastern Mediterranean. This anti-correlation partly results from the convective uplift of freshly polluted air masses rich in CO but poor in O_3 and of the subsidence of O_3-enriched and CO poor air masses in the subsidence region in the western part of the domain.

In order to quantify the impact of the different emission sources on the Asian upper troposphere CO and O_3 budget, we performed sensitivity simulations with CO and NOx sources switched off by type and region and one simulation with tagged stratospheric O_3. For CO, it appears that South-Asia is the most important contributor ($\sim$25 ppbv) to filling up the AMA because emissions (the IGP), convection and upper-level anticyclone coincide. East-Asia is more polluted than South-Asia but convection in this region is less strong than in South-Asia and does not uplift pollution deep enough into the upper-troposphere to contribute significantly to the AMA CO filling ($\sim$10 ppbv). For the same reason, NOx from South Asian pollution sources contribute more to the O_3 formation within the anticyclone ($\sim$8 ppbv) than NOx from China ($\sim$5 ppbv). Nevertheless, LiNOx from Asia are the most important contributor to the photochemical O_3 formation within the AMA with a production which is up to two times larger (10- 14 ppbv) than South Asian pollution. Finally, STE plays an important role for O_3 in the upper part of the AMA (above 150 hPa) with a contribution (7-10 ppbv) which is probably overestimated because of the stratospheric O_3 overestimation by the model.

Acknowledgements. IASI L1c and L2–EUMETSAT data have been downloaded from the Ether French atmospheric database (http://ether.ipsl.jussieu.fr). The research with IASI is conducted with financial support from the CNES (TOSCA–IASI project). MOZAIC is presently funded by INSU–CNRS, Météo–France, and FZJ (Forschungszentrum Julich, Germany). The MOZAIC-MOZAIC data are available via http://www.iagos.fr/web/, thanks to the support from Ether. MERRA data used in this study were provided by the Global Modeling and Assimilation Office (GMAO) at NASA Goddard Space Flight Center through the NASA GES DISC online archive.

References

References

Barret, B., Turquety, S., Hurtmans, D., Clerbaux, C., Hadji-Lazaro, J., Bey, I., Auvray, M., and Coheur, P.: Global carbon monoxide vertical distributions from spaceborne high-resolution FTIR nadir measurements, Atmospheric Chemistry and Physics, 5, 2901–2914, 2005.

Barret, B., Ricaud, P., Mari, C., Attie, J. L., Bousserez, N., Josse, B., Le Flochmoen, E., Livesey, N. J., Massart, S., Peuch, V. H., Piacentini, A., Sauvage, B., Thouret, V., and Cammas, J. P.: Transport pathways of CO in the African upper troposphere during the monsoon season: a study based upon the assimilation of spaceborne observations, Atmospheric Chemistry and Physics, 8, 3231–3246, 2008.

Barret, B., Williams, J. E., Bouarar, I., Yang, X., Josse, B., Law, K., Pham, M., Le Flochmoen, E., Liousse, C., Peuch, V. H., Carver, G. D., Pyle, J. A., Sauvage, B., van Velthoven, P., Schlager, H., Mari, C., and Cammas, J. P.: Impact of West African Monsoon convective transport and lightning NOx production upon the upper tropospheric composition: a multi-model study, Atmospheric Chemistry and Physics, 10, 5719–5738, doi:10.5194/acp-10-5719-2010, 2010.

Barret, B., Le Flochmoen, E., Sauvage, B., Pavelin, E., Matricardi, M., and Cammas, J. P.: The detection of post-monsoon tropospheric ozone variability over south Asia using IASI data, Atmospheric Chemistry and Physics, 11, 9533–9548, doi:10.5194/acp-11-9533-2011, 2011.

Bergman, J. W., Fierli, F., Jensen, E. J., Honomichl, S., and Pan, L. L.: Boundary layer sources for the Asian anticyclone: Regional contributions to a vertical conduit, Journal of Geophysical Research-Atmospheres, 118, 2560–2575, doi:10.1002/jgrd.50142, 2013.

Bey, I., Jacob, D. J., Logan, J. A., and Yantosca, R. M.: Asian chemical outflow to the Pacific in spring: Origins, pathways, and budgets, Journal of Geophysical Research-Atmospheres, 106, 23 097–23 113, doi:10.1029/2001jd000806, 2001.

Chen, W.-T., Liao, H., and Seinfeld, J. H.: Future climate impacts of direct radiative forcing of anthropogenic aerosols, tropospheric ozone, and long-lived greenhouse gases, Journal of Geophysical Research-Atmospheres, 112, doi:10.1029/2006jd008051, 2007.

Clerbaux, C., Boynard, A., Clarisse, L., George, M., Hadji-Lazaro, J., Herbin, H., Hurtmans, D., Pommier, M., Razavi, A., Turquety, S., Wespes, C., and Coheur, P. F.: Monitoring of atmospheric composition using the thermal infrared IASI/MetOp sounder, Atmospheric Chemistry and Physics, 9, 6041–6054, 2009.

Cristofanelli, P., Bracci, A., Sprenger, M., Marinoni, A., Bonafe, U., Calzolari, F., Duchi, R., Laj, P., Pichon, J., Roccato, F., Venzac, H., Vuillermoz, E., and Bonasoni, P.: Tropospheric ozone variations at the Nepal Climate Observatory-Pyramid (Himalayas, 5079 m a.s.l.) and influence of deep stratospheric intrusion events, Atmospheric Chemistry and Physics, 10, 6537–6549, doi:doi:10.5194/acp-10-6537-2010, 2010.

De Wachter, E., Barret, B., Le Flochmoen, E., Pavelin, E., Matricardi, M., Clerbaux, C., Hadji-Lazaro, J., George, M., Hurtmans, D., Coheur, P. F., Nedelec, P., and Cammas, J. P.: Retrieval of MetOp-A/IASI CO profiles and validation with MOZAIC data, Atmospheric Measurement Techniques, 5, 2843–2857, doi:10.5194/amt-5-2843-2012, 2012.

Doherty, R. M., Stevenson, D. S., Collins, W. J., and Sanderson, M. G.: Influence of convective transport on tropospheric ozone and its precursors in a chemistry-climate model, Atmospheric Chemistry and Physics, 5, 3205–3218, 2005.

Dufour, G., Eremenko, M., Griesfeller, A., Barret, B., LeFlochmoen, E., Clerbaux, C., Hadji-Lazaro, J., Coheur, P. F., and Hurtmans, D.: Validation of three different scientific ozone products retrieved from IASI spectra using ozonesondes, Atmospheric Measurement Techniques, 5, 611–630, doi:10.5194/amt-5-611-2012, 2012.

Eastham, S. D., Weisenstein, D. K., and Barrett, S. R. H.: Development and evaluation of the unified tropospheric-stratospheric chemistry extension (UCX) for the global chemistry-transport model GEOS-Chem, Atmospheric Environment, 89, 52–63, doi:10.1016/j.atmosenv.2014.02.001, 2014.

Eremenko, M., Dufour, G., Foret, G., Keim, C., Orphal, J., Beekmann, M., Bergametti, G., and Flaud, J. M.: Tropospheric ozone distributions over Europe during the heat wave in July 2007 observed from infrared nadir spectra recorded by IASI, Geophysical Research Letters, 35, doi:10.1029/2008gl034803, 2008.

Fiore, A., Jacob, D., Bey, I., Yantosca, R., Field, B., Fusco, A., and Wilkinson, J.: Background ozone over the United States in summer: Origin, trend, and contribution to pollution episodes, Journal of Geophysical Research-Atmospheres, 107, doi:10.1029/2001JD000982, 2002.

Garny, H. and Randel, W.: Dynamic variability of the Asian monsoon anticyclone observed in potential vorticity and correlations with tracer distributions, Journal of Geophysical Research-Atmospheres, 118, 13 421–13 433, doi:10.1002/2013JD020908, 2013.

George, M., Clerbaux, C., Hurtmans, D., Turquety, S., Coheur, P. F., Pommier, M., Hadji-Lazaro, J., Edwards, D. P., Worden, H., Luo, M., Rinsland, C., and McMillan, W.: Carbon monoxide distributions from the IASI/METOP mission: evaluation with other space-borne remote sensors, Atmospheric Chemistry and Physics, 9, 8317–8330, 2009.

Heath, N. K. and Fuelberg, H. E.: Using a WRF simulation to examine regions where convection impacts the Asian summer monsoon anticyclone, Atmospheric Chemistry and Physics, 14, 2055–2070, doi:10.5194/acp-14-2055-2014, 2014.

Hoskins, B. J. and Rodwell, M. J.: A Model of the Asian Summer Monsoon. Part I: The Global Scale, Journal of the Atmospheric Sciences, 52, 1329–1340, 1995.

Jacob, D. J., Heikes, B. G., Fan, S. M., Logan, J. A., Mauzerall, D. L., Bradshaw, J. D., Singh, H. B., Gregory, G. L., Talbot, R. W., Blake, D. R., and Sachse, G. W.: Origin of ozone and NOx in the tropical troposphere: A photochemical analysis of aircraft observations over the South Atlantic basin, Journal of Geophysical Research-Atmospheres, 101, 24 235–24 250, doi:10.1029/96jd00336, 1996.

Kar, J., Bremer, H., Drummond, J. R., Rochon, Y. J., Jones, D. B. A., Nichitiu, F., Zou, J., Liu, J., Gille, J. C., Edwards, D. P., Deeter, M. N., Francis, G., Ziskin, D., and Warner, J.: Evidence of vertical transport of carbon monoxide from Measurements of Pollution in the Troposphere (MOPITT), Geophysical Research Letters, 31, doi:10.1029/2004gl021128, 2004.

Kunhikrishnan, T., Lawrence, M. G., von Kuhlmann, R., Richter, A., Ladstatter-Weissenmayer, A., and Burrows, J. P.: Analysis of tropospheric NOx over Asia using the model of atmospheric transport and chemistry (MATCH-MPIC) and GOME-satellite observations, Atmospheric Environment, 38, 581–596, doi:10.1016/j.atmosenv.2003.09.074, 2004.

Kunhikrishnan, T., Lawrence, M. G., von Kuhlmann, R., Wenig, M. O., Asman, W. A. H., Richter, A., and Burrows, J. P.: Regional NOx emission strength for the Indian subcontinent and the impact of emis-

sions from India and neighboring countries on regional O-3 chemistry, Journal of Geophysical Research-Atmospheres, 111, doi:10.1029/2005jd006036, 2006.

Lawrence, M. G., von Kuhlmann, R., Salzmann, M., and Rasch, P. J.: The balance of effects of deep convective mixing on tropospheric ozone, Geophysical Research Letters, 30, doi:10.1029/2003gl017644, 2003.

Li, Q. B., Jacob, D. J., Logan, J. A., Bey, I., Yantosca, R. M., Liu, H. Y., Martin, R. V., Fiore, A. M., Field, B. D., Duncan, B. N., and Thouret, V.: A tropospheric ozone maximum over the Middle East, Geophysical Research Letters, 28, 3235–3238, doi:10.1029/2001gl013134, 2001.

Li, Q. B., Jiang, J. H., Wu, D. L., Read, W. G., Livesey, N. J., Waters, J. W., Zhang, Y. S., Wang, B., Filipiak, M. J., Davis, C. P., Turquety, S., Wu, S. L., Park, R. J., Yantosca, R. M., and Jacob, D. J.: Convective outflow of South Asian pollution: A global CTM simulation compared with EOS MLS observations, Geophysical Research Letters, 32, 4, doi:10.1029/2005gl022762, 2005.

Liousse, C., Guillaume, B., Grégoire, J. M., Mallet, M., Galy, C., Pont, V., Akpo, A., Bedou, M., Castéra, P., Dungall, L., Gardrat, E., Granier, C., Konare, A., Malavelle, F., Mariscal, A., Mieville, A., Rosset, R., Serça, D., Solmon, F., Tummon, F., Assamoi, E., Yoboué, V., and Van Velthoven, P.: Updated African biomass burning emission inventories in the framework of the AMMA-IDAF program, with an evaluation of combustion aerosols, Atmos. Chem. Phys., 10, 9631–9646, doi:10.5194/acp-10-9631-2010, 2010.

Liu, J., Logan, J. A., Murray, L. T., Pumphrey, H. C., Schwartz, M. J., and Megretskaia, I. A.: Transport analysis and source attribution of seasonal and interannual variability of CO in the tropical upper troposphere and lower stratosphere, Atmospheric Chemistry and Physics, 13, 129–146, doi:10.5194/acp-13-129-2013, 2013.

Liu, J. H., Logan, J. A., Jones, D. B. A., Livesey, N. J., Megretskaia, I., Carouge, C., and Nedelec, P.: Analysis of CO in the tropical troposphere using Aura satellite data and the GEOS-Chem model: insights into transport characteristics of the GEOS meteorological products, Atmospheric Chemistry and Physics, 10, 12 207–12 232, doi:10.5194/acp-10-12207-2010, 2010.

Liu, J. J., Jones, D. B. A., Worden, J. R., Noone, D., Parrington, M., and Kar, J.: Analysis of the summertime buildup of tropospheric ozone abundances over the Middle East and North Africa as observed by the Tropospheric Emission Spectrometer instrument, Journal of Geophysical Research-Atmospheres, 114, doi:10.1029/2008jd010993, 2009.

Marenco, A., Thouret, V., Nedelec, P., Smit, H., Helten, M., Kley, D., Karcher, F., Simon, P., Law, K., Pyle, J., Poschmann, G., Von Wrede, R., Hume, C., and Cook, T.: Measurement of ozone and water vapor by Airbus in-service aircraft: The MOZAIC airborne program, An overview, Journal of Geophysical Research-Atmospheres, 103, 25 631–25 642, doi:10.1029/98jd00977, 1998.

Martin, R. V., Jacob, D., Logan, J., Bey, I., Yantosca, R., Staudt, A., Li, Q., Fiore, A., Duncan, B., Liu, H., Ginoux, P., and Thouret, V.: Interpretation of TOMS observations of tropical tropospheric ozone with a global model and in-situ observations, Journal of Geophysical Research-Atmospheres, 107, doi:10.1029/2001JD001480, 2002.

Martin, R. V., Sauvage, B., Folkins, I., Sioris, C. E., Boone, C., Bernath, P., and Ziemke, J.: Space-based constraints on the production of nitric oxide by lightning, Journal of Geophysical Research-Atmospheres, 112, doi:10.1029/2006jd007831, 2007.

McLinden, C. A., Olsen, S. C., Hannegan, B., Wild, O., Prather, M. J., and Sundet, J.: Stratospheric ozone in 3-D models: A simple chemistry and the cross-tropopause flux, Journal of Geophysical Research-Atmospheres, 105, 14 653–14 665, doi:10.1029/2000jd900124, 2000.

Moorthi, S. and Suarez, M. J.: RELAXED ARAKAWA-SCHUBERT - A PARAMETERIZATION OF MOIST CONVECTION FOR GENERAL-CIRCULATION MODELS, Monthly Weather Review, 120, 978–1002, doi:10.1175/1520-0493(1992)120<0978:rasapo>2.0.co;2, 1992.

Murray, L., Jacob, D., Logan, J., Hudman, R., and Koshah, W.: Optimized regional and interannual variability of lightning in a global chemical transport model constrained by LIS/OTD satellite data, Journal of Geophysical Research-Atmospheres, 117, 2012.

Nassar, R., Logan, J. A., Megretskaia, I. A., Murray, L. T., Zhang, L., and Jones, D. B. A.: Analysis of tropical tropospheric ozone, carbon monoxide, and water vapor during the 2006 El Nino using TES observations and the GEOS-Chem model, Journal of Geophysical Research-Atmospheres, 114, doi:10.1029/2009jd011760, 2009.

Nedelec, P., Cammas, J. P., Thouret, V., Athier, G., Cousin, J. M., Legrand, C., Abonnel, C., Lecoeur, F., Cayez, G., and Marizy, C.: An improved infrared carbon monoxide analyser for routine measurements aboard commercial Airbus aircraft: technical validation and first scientific results of the MOZAIC III programme, Atmospheric Chemistry and Physics, 3, 1551–1564, 108, 2003.

Park, M., Randel, W. J., Gettelman, A., Massie, S. T., and Jiang, J. H.: Transport above the Asian summer monsoon anticyclone inferred from Aura Microwave Limb Sounder tracers, Journal of Geophysical Research-Atmospheres, 112, doi:10.1029/2006jd008294, 2007.

Park, M., Randel, W. J., Emmons, L. K., Bernath, P. F., Walker, K. A., and Boone, C. D.: Chemical isolation in the Asian monsoon anticyclone observed in Atmospheric Chemistry Experiment (ACE-FTS) data, Atmospheric Chemistry and Physics, 8, 757–764, 2008.

Park, M., Randel, W. J., Emmons, L. K., and Livesey, N. J.: Transport pathways of carbon monoxide in the Asian summer monsoon diagnosed from Model of Ozone and Related Tracers (MOZART), Journal of Geophysical Research-Atmospheres, 114, doi:10.1029/2008jd010621, 2009.

Ploeger, F., Gottschling, C., Griessbach, S., Grooß, J.-U., Guenther, G., Konopka, P., Müller, R., Riese, M., Stroh, F., Tao, M., Ungermann, J., Vogel, B., and von Hobe, M.: A potential vorticity-based determination of the transport barrier in the Asian summer monsoon anticyclone, Atmospheric Chemistry and Physics, 15, 13 145–13 159, doi:10.5194/acp-15-13145-2015, 2015.

Popovic, J. M. and Plumb, R. A.: Eddy shedding from the upper-tropospheric Asian monsoon anticyclone, Journal of the Atmospheric Sciences, 58, 93–104, doi:10.1175/1520-0469(2001)058<0093:esftut>2.0.co;2, 2001.

Price, C. and Rind, D.: Modeling global lightning distributions in a general circulation model, Monthly Weather Review, pp. 1930–1932, doi:10.1175/1520-0493, 1994.

Randel, W. J. and Park, M.: Deep convective influence on the Asian summer monsoon anticyclone and associated tracer variability observed with Atmospheric Infrared Sounder (AIRS), Journal of Geophysical Research-Atmospheres, 111, doi:10.1029/2005jd006490, 2006.

Randel, W. J., Park, M., Emmons, L., Kinnison, D., Bernath, P., Walker, K. A., Boone, C., and Pumphrey, H.: Asian Monsoon Transport of Pollution to the Stratosphere, Science, 328, 611–613, doi:10.1126/science.1182274, 2010.

Rodgers, C. D.: Inverse methods for atmospheric sounding: Theory and Practice, Series on Atmospheric, Oceanic and Planetary Physics - Vol. 2, World Scientific, Singapore, New Jersey, London, Hong Kong, 238pp., 2000.

Sauvage, B., Thouret, V., Cammas, J. P., Gheusi, F., Athier, G., and Nedelec, P.: Tropospheric ozone over Equatorial Africa: regional aspects from the MOZAIC data, Atmospheric Chemistry and Physics, 5, 311–335, doi:10.5194/acp-5-311-2005, 2005.

Sauvage, B., Martin, R. V., van Donkelaar, A., Liu, X., Chance, K., Jaegle, L., Palmer, P. I., Wu, S., and Fu, T. M.: Remote sensed and in situ constraints on processes affecting tropical tropospheric ozone, Atmospheric Chemistry and Physics, 7, 815–838, 2007a.

Sauvage, B., Martin, R. V., van Donkelaar, A., and Ziemke, J. R.: Quantification of the factors controlling tropical tropospheric ozone and the South Atlantic maximum, Journal of Geophysical Research-Atmospheres, 112, doi:10.1029/2006jd008008, 2007b.

Schumann, U. and Huntrieser, H.: The global lightning-induced nitrogen oxides source, Atmospheric Chemistry and Physics, 7, 3823–3907, 2007.

Shindell, D. T., Faluvegi, G., Stevenson, D. S., Krol, M. C., Emmons, L. K., Lamarque, J. F., Petron, G., Dentener, F. J., Ellingsen, K., Schultz, M. G., Wild, O., Amann, M., Atherton, C. S., Bergmann, D. J., Bey, I., Butler, T., Cofala, J., Collins, W. J., Derwent, R. G., Doherty, R. M., Drevet, J., Eskes, H. J., Fiore, A. M., Gauss, M., Hauglustaine, D. A., Horowitz, L. W., Isaksen, I. S. A., Lawrence, M. G., Montanaro, V., Mueller, J. F., Pitari, G., Prather, M. J., Pyle, J. A., Rast, S., Rodriguez, J. M., Sanderson, M. G., Savage, N. H., Strahan, S. E., Sudo, K., Szopa, S., Unger, N., van Noije, T. P. C., and Zeng, G.: Multimodel simulations of carbon monoxide: Comparison with observations and projected near-future changes, Journal of Geophysical Research-Atmospheres, 111, doi:10.1029/2006jd007100, 2006.

Streets, D. G., Yu, C., Bergin, M. H., Wang, X. M., and Carmichael, G. R.: Modeling study of air pollution due to the manufacture of export goods in China's Pearl River Delta, Environmental Science and Technology, 40, 2099–2107, doi:10.1021/es051275n, 2006.

Thouret, V., Marenco, A., Logan, J. A., Nedelec, P., and Grouhel, C.: Comparisons of ozone measurements from the MOZAIC airborne program and the ozone sounding network at eight locations, Journal of Geophysical Research-Atmospheres, 103, 25 695–25 720, doi:10.1029/98jd02243, 1998.

Tocquer, F., Barret, B., Mari, C., Le Flochmoen, E., Cammas, J.-P., and Sauvage, B.: An upper tropospheric 'ozone river' from Africa to India during the 2008 Asian post-monsoon season, Tellus Series B-Chemical and Physical Meteorology, 67, doi:10.3402/tellusb.v67.25350, 2015.

van der Werf, G. R., Randerson, J. T., Giglio, L., Collatz, G. J., Mu, M., Kasibhatla, P. S., Morton, D. C., DeFries, R. S., Jin, Y., and van Leeuwen, T. T.: Global fire emissions and the contribution of deforestation, savanna, forest, agricultural, and peat fires (1997-2009), Atmospheric Chemistry and Physics, 10, 11 707–11 735, doi:10.5194/acp-10-11707-2010, 2010.

Table 1. Statistics of GC versus IASI UTLS CO and O_3 columns comparison over the 10°S-40°N and 0-160°E domain for monthly averages during the MJJASO period. Figures are given for GC profiles smoothed with the averaging kernels (GCwAvK) and figures in italic between brackets correspond to GC raw data.

	r	Bias %	Std. Dev. %
CO	0.70 *(0.59)*	-11.2 *(-11.4)*	9.4 *(11.8)*
O_3	0.94 *(0.93)*	-13.8 *(-19.6)*	26.5 *(32.8)*

Table 2. Monthly CO from different sources inside and outside of the AMA in ppbv.

	Anthropic East Asia		Anthropic South Asia	
	AMA	Out	AMA	Out
June	8.3	5.3	17.3	10.1
July	10.7	8.9	25.3	13.8
August	9.9	10.0	23.7	15.9
September	7.8	7.4	14.3	8.2

Vogel, B., Gunther, G., Muller, R., Grooß, J.-U., , and Riese, M.: Impact of different Asian source regions on the composition of the Asian monsoon anticyclone and of the extratropical lowermost stratosphere, Atmospheric Chemistry and Physics, 15, 13 699–13 716, doi:10.5194/acp-15-13699-2015, 2015.

Wu, S., Mickley, L., Jacob, D., Logan, J., Yantosca, R., and Rind, D.: Why are there large differences between models in global budgets of tropospheric ozone?, Journal of Geophysical Atmosphere, 112, doi:10.1029/2006JD007801, 2007.

Yamasoe, M. A., Sauvage, B., Thouret, V., Nédélec, P., Le Flochmoen, E., and Barret, B.: Analysis of tropospheric ozone and carbon monoxide profiles over South America based on MOZAIC/IAGOS database and model simulations, Tellus-B, p. accepted, 2015.

Yan, R. and Bian, J.: Tracing the boundary layer sources of carbon monoxide in the Asian summer monsoon anticyclone using WRF-Chem, Advances in Atmospheric Sciences, 32, 943–951, doi:10.1007/s00376-014-4130-3, 2015.

Zhang, Q., Wu, G., and Qian, Y.: Asia high and its relationship to the climate anomaly over East Asia in summer, J. Meteorol. Soc. Jpn., 80, 733–744, 2002.

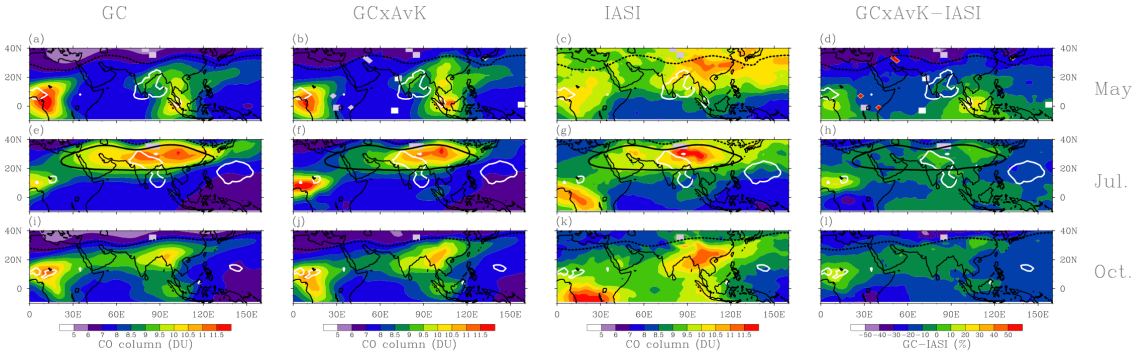

Figure 1. Distributions of UTLS (270-110 hPa) CO columns: (a,e,i) GEOS-Chem, (b,f,j) GEOS-Chem smoothed with IASI AvK, (c,g,k) IASI and (d,h,l) relative differences between GC smoothed with IASI AvK and IASI. From top to bottom, panels correspond to monthly periods with (a,b,c,d) May, (e,f,g,h) July, (i,j,k,l) October. The white solid line represents the 2.5 kg/m^2/s Convective Upward Mass Flux from GEOS-5 averaged over 350-150 hPa. The black dashed line is the tropopause (2PVU) and the black solid line is the 12520 m GH representing the AMA boundary at 200 hPa.

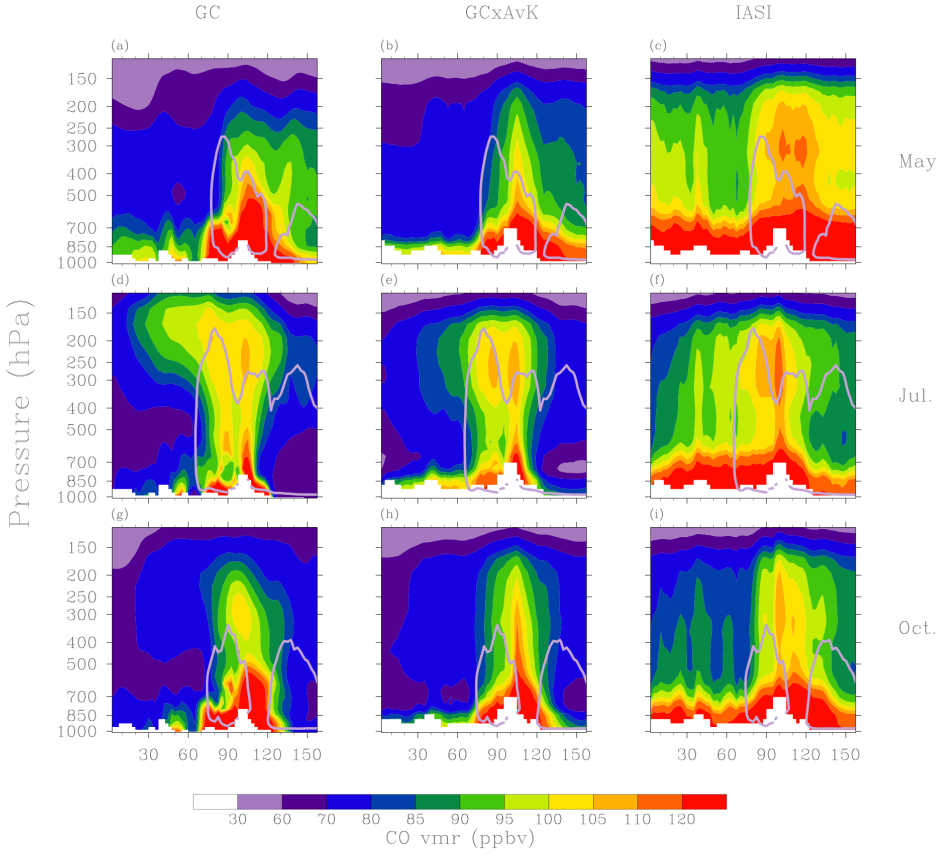

Figure 2. Longitude-Pressure cross-sections of CO mixing ratios averaged over 23-29°N: (a,d,g) GEOS-Chem, (b,e,h) GEOS-Chem smoothed with IASI averaging kernels (c,f,i) IASI. From top to bottom, panels correspond to monthly periods with (a,b,c) May, (d,e,f) July, (g,h,i) October. The grey solid line represents the 2.5 kg/m^2/s Convective Upward Mass Flux from GEOS-5.

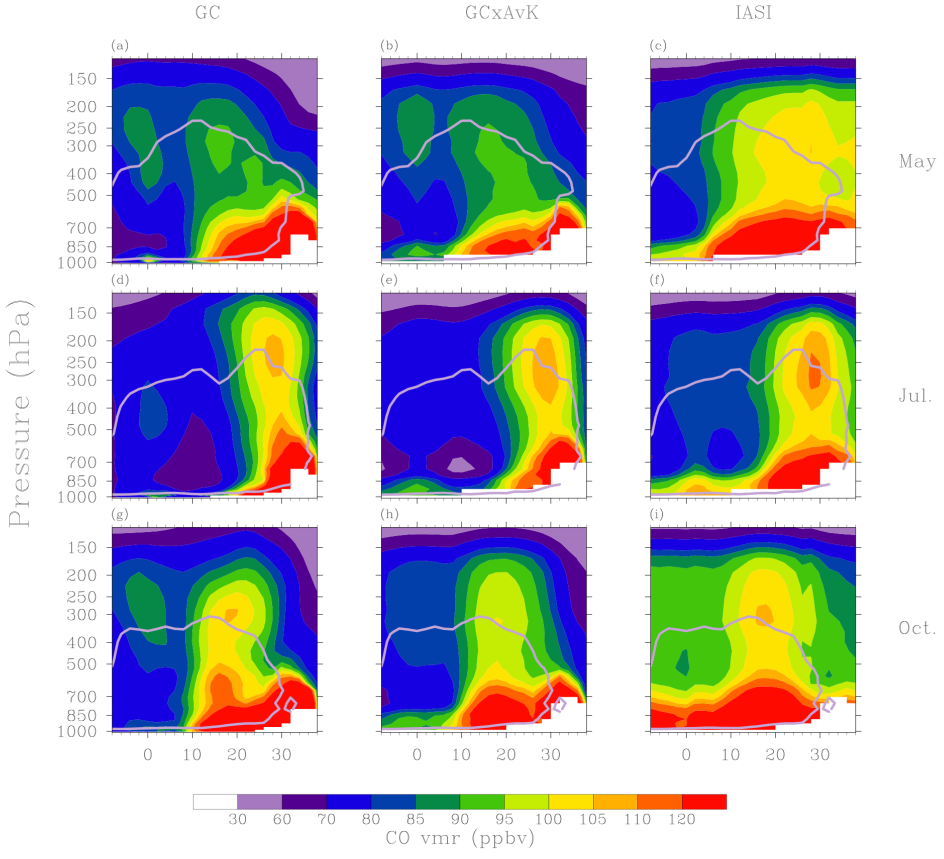

Figure 3. Latitude-Pressure cross-sections of CO mixing ratios averaged over 75-105°E: (a,d,g) GEOS-Chem, (b,e,h) GEOS-Chem smoothed with IASI averaging kernels (c,f,i) IASI. From top to bottom, panels correspond to monthly periods with (a,b,c) May, (d,e,f) July, (g,h,i) October. The grey solid line represents the 2.5 kg/m^2/s Convective Upward Mass Flux from GEOS-5.

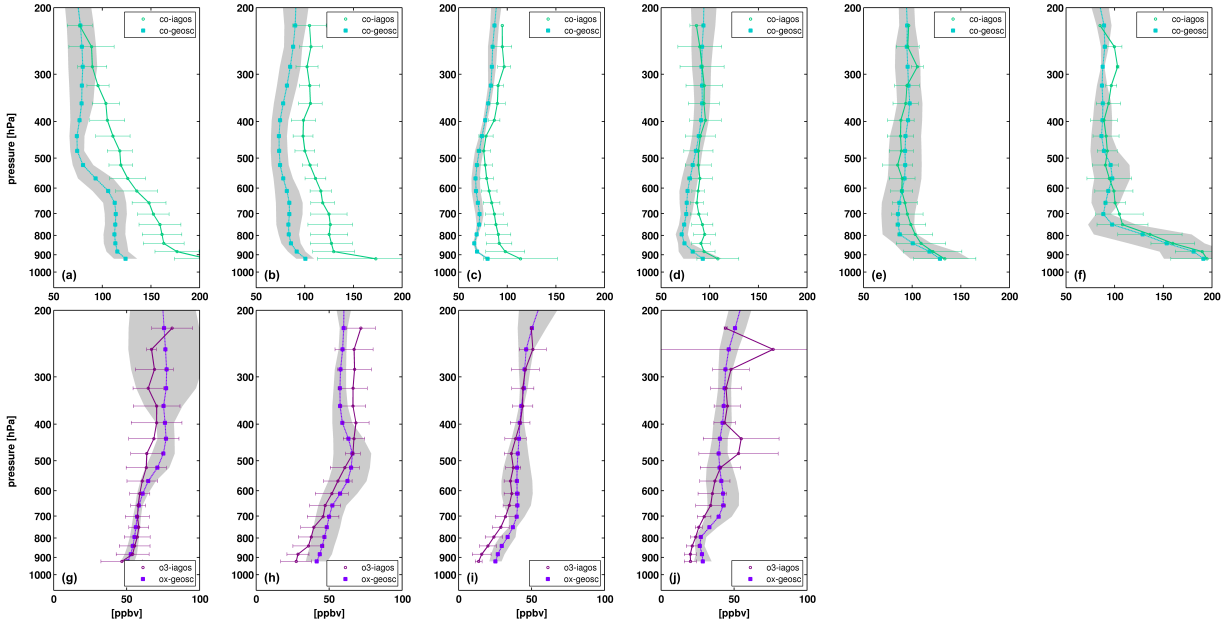

Figure 4. Monthly mean tropospheric vertical profiles of CO and O_3 at Hyderabad (17.2°N, 78.3°E) from MOZAIC-MOZAIC airborne observations and GEOS-Chem simulations. Top panels: CO from May to October 2009, Bottom panels: O_3 from May to August 2009. The grey shadings and the error bars represent the 1-σ variability for GC and MOZAIC respectively.

Table 3. Monthly O_3 and NOx from different sources inside and outside of the AMA in ppbv. The values for NOx are given in brackets.

	Anthropic East Asia		Anthropic South Asia		LiNOx Asia		LiNOx Africa		Strato.	
	AMA	Out	AMA	Out	AMA	Out	AMA	Out	AMA	Out
June	3.3	2.0	4.6	2.0	9.5	6.3	3.6	5.4	11.8	9.6
	(0.027)	(0.010)	(0.025)	(0.012)	(0.11)	(0.05)	(0.019)	(0.005)		
July	5.2	4.6	7.6	4.7	13.5	7.2	1.0	1.5	10.0	5.9
	(0.033)	(0.021)	(0.043)	(0.017)	(0.129)	(0.048)	(0.012)	(0.018)		
August	4.9	5.2	8.1	4.4	9.9	5.3	0.9	1.2	6.7	3.9
	(0.027)	(0.023)	(0.042)	(0.016)	(0.087)	(0.036)	(0.011)	(0.022)		
September	3.4	3.3	5.2	4.0	6.1	5.0	1.1	2.2	6.7	4.7
	(0.018)	(0.014)	(0.033)	(0.018)	(0.074)	(0.044)	(0.010)	(0.032)		

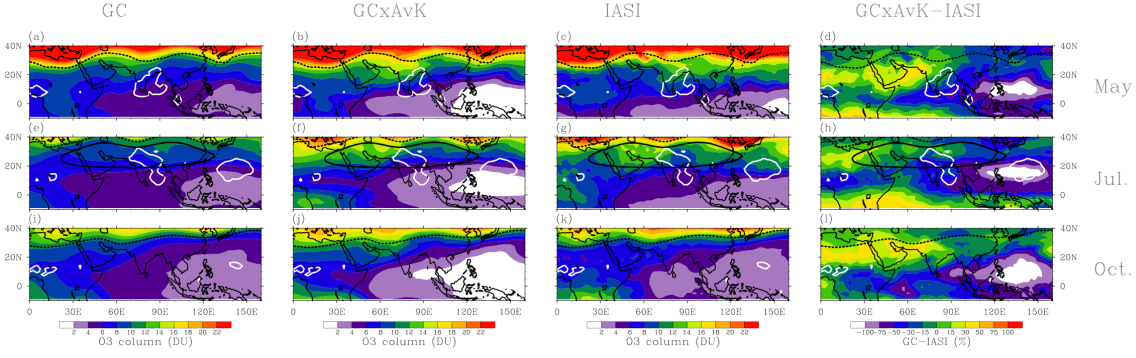

Figure 5. Same as Figure 1 for O_3.

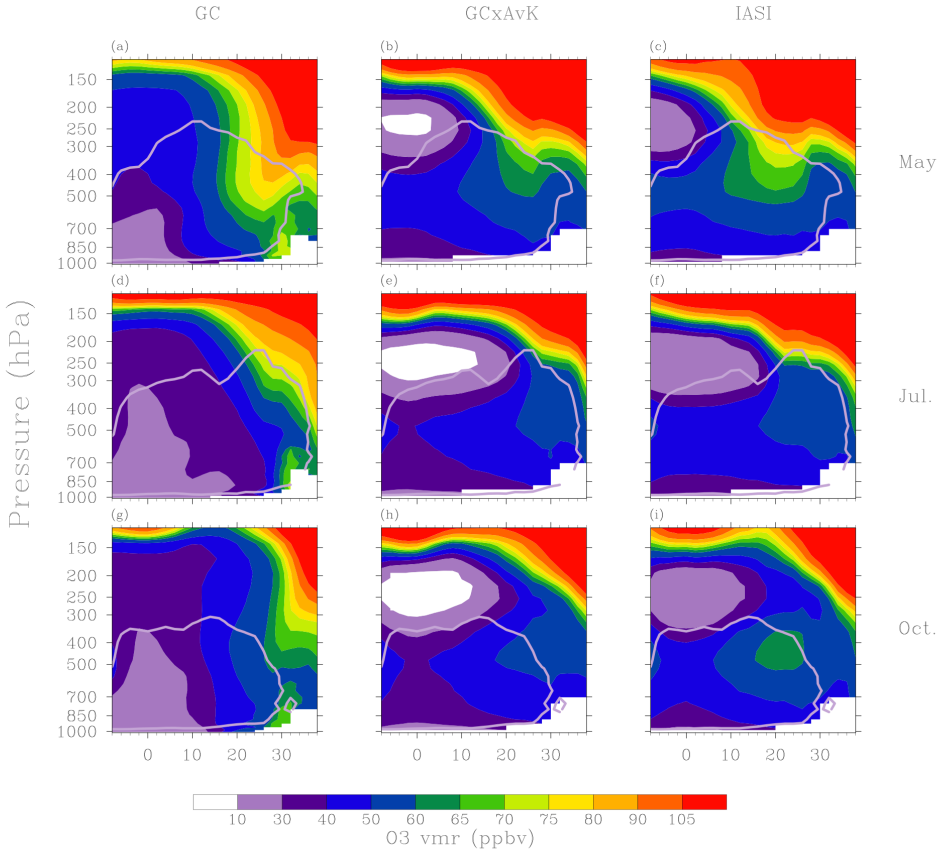

Figure 6. Same as Figure 3 for O_3.

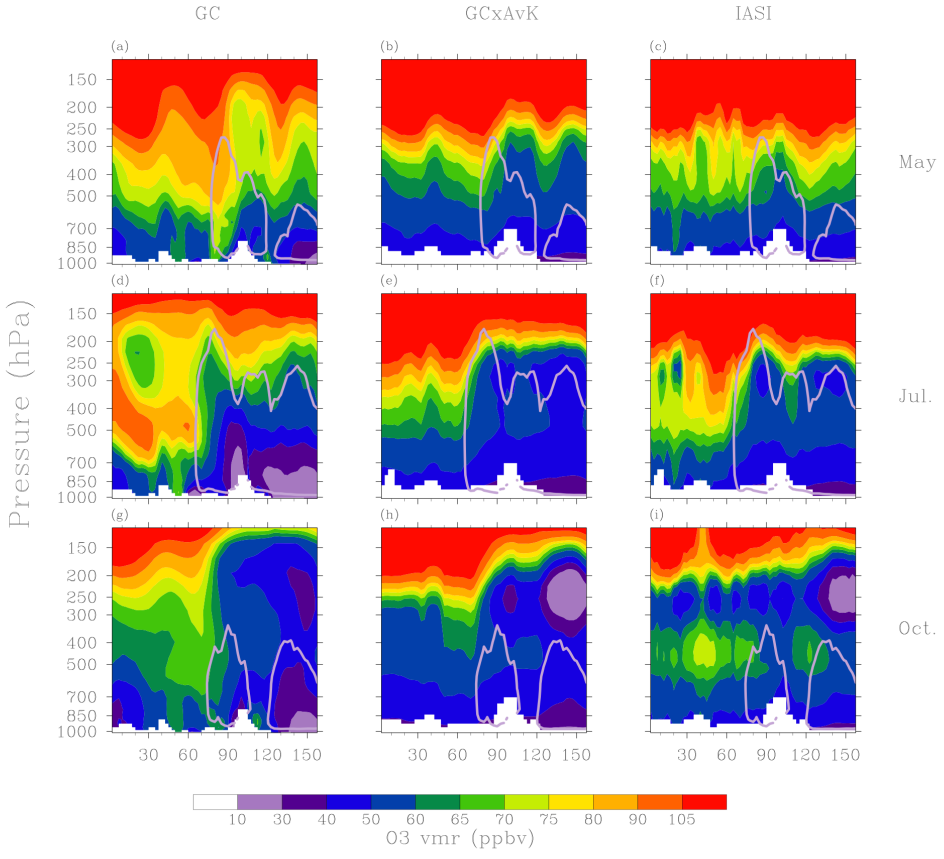

Figure 7. Same as Figure 2 for O_3.

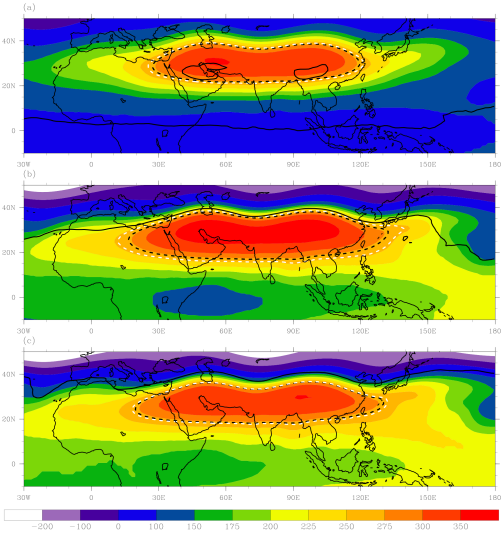

Figure 8. Geopotential heights (GH) from MERRA for July 2009 at (a) 100 (b) 150 hPa and (c) 200 hPa. The black dotted lines represent the GH isocontours at (a) 16770 m (b) 14350 m and (c) 12520 m and the white dotted line represents the 270 m GH anomalies (see text for details).

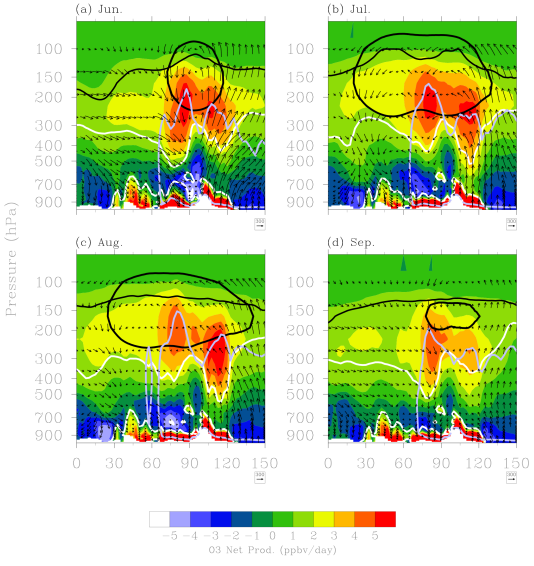

Figure 9. Longitude-pressure cross-sections of GC simulated O_3 net production rates averaged over 23-29°N in (a) June, (b) July, (c) August and (d) September 2009. The black arrows correspond to the O_3 fluxes and the white solid lines to the 100 pptv NOx contours from GC. The dashed black line corresponds to the tropopause (2 PVU), the grey solid line to upward convective mass fluxes of 2.5 kg/m^2/s at 200 hPa and the black solid line to the AMA boundary computed as the 270 m GH anomaly (see text for details).

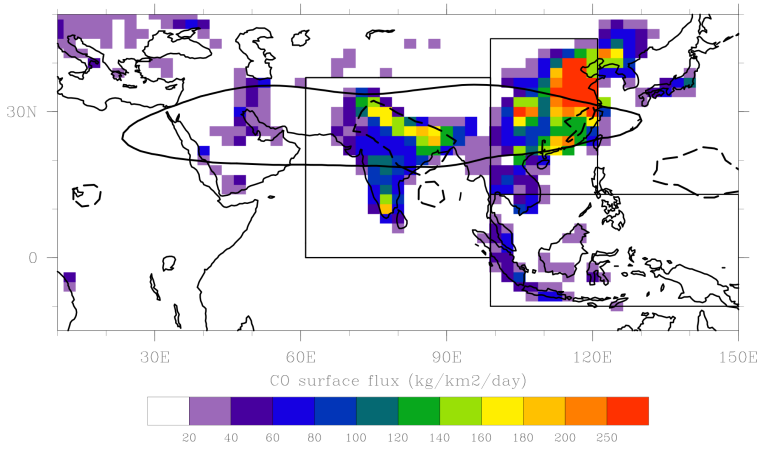

Figure 10. Anthropogenic emissions of CO from the Streets 2006 inventory for July. The black dashed line is the 2.5 kg/m^2/s Convective Upward Mass Flux contour at 2225 hPa from GEOS-5 for July 2009 and the solid black line is the 12520 m GH contour from MERRA at 200 hPa for July 2009. The 3 boxes correspond to the regions selected for the sensitivity simulations with anthropogenic emissions switched off (South, East and South-East Asia).

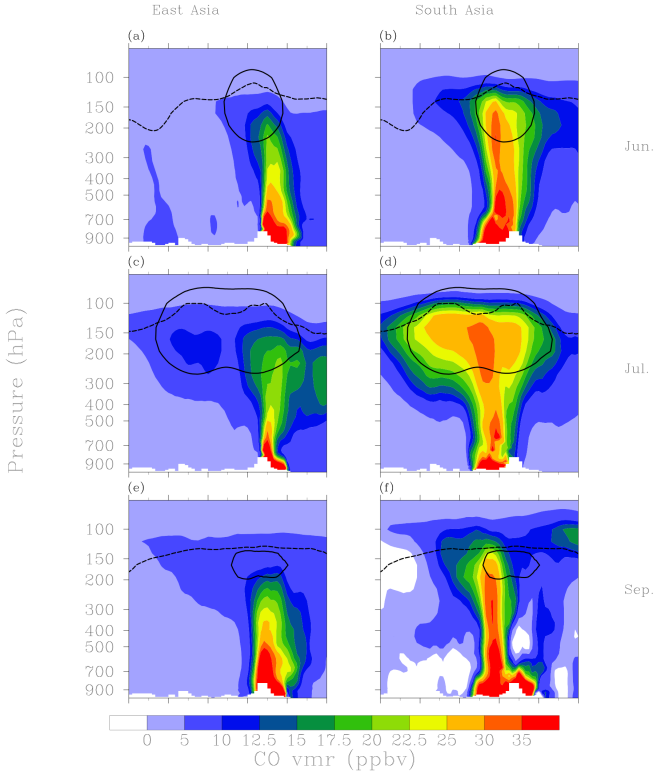

Figure 11. Longitude pressure cross sections of the sensitivity of CO to anthropogenic CO sources averaged over 23-29°N from (a,c,e) East Asia (b, d,f) South Asia computed as the differences between the control run and simulations with the corresponding source switched off. From top to bottom, panels correspond to (a,b) June, (c,d) July and (e,f) September 2009.

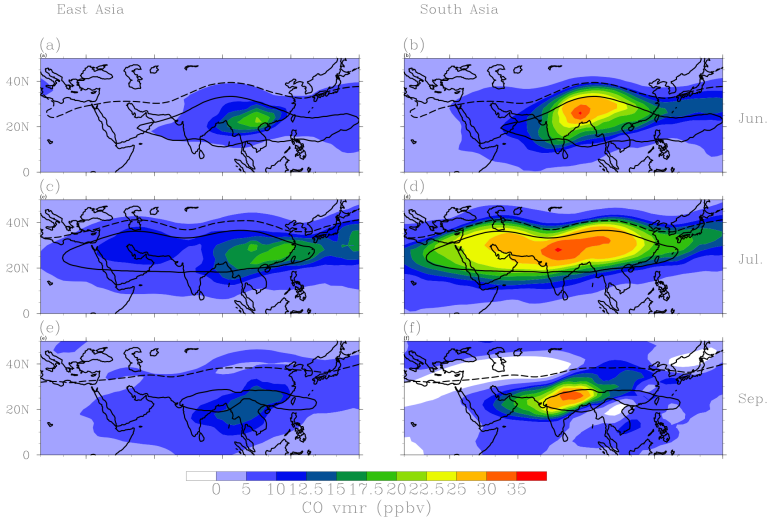

Figure 12. Same as in Fig. 11 for the distributions at 200 hPa.

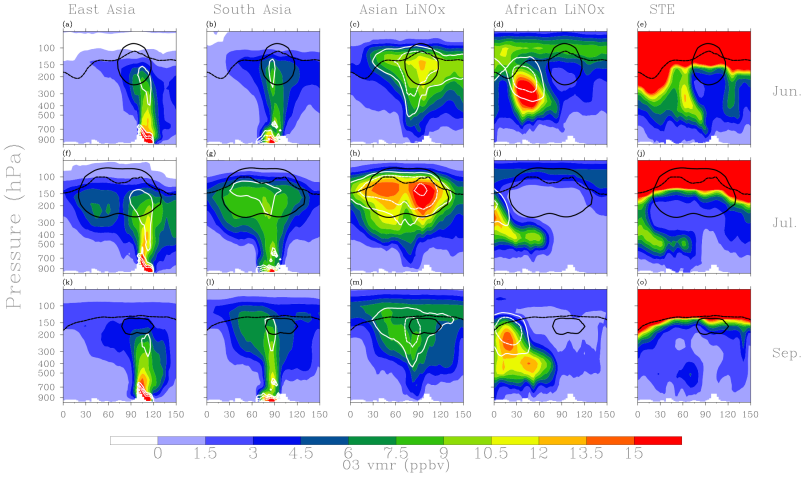

Figure 13. Longitude pressure cross sections of the sensitivity of O_3 to NOx sources averaged over 23-29°N for: (a,f,k) East Asian anthropogenic (b,g,l) South Asian anthropogenic (c,h,m) Asian lightning (d,i,n) African lightning computed as the difference between the control run and simulations with the corresponding source switched off. Panels (e,j,o) correspond to tagged stratospheric O_3 to diagnose STE. From top to bottom, panels correspond to monthly means with (a,b,c,d,e) June, (f,g,h,i,j) July and (k,l,m,n,o) September 2009. The white solid, dashed and dotted lines correspond to the 50, 100 and 200 pptv contours for the sensitivity of NOx to the different NOx sources.

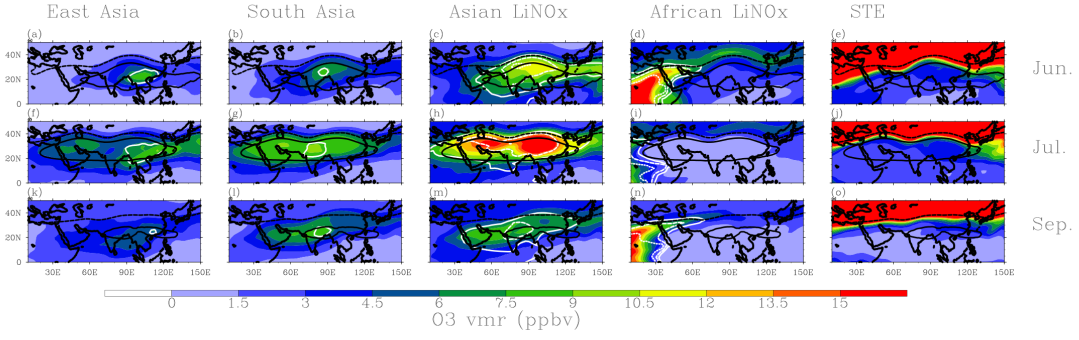

Figure 14. Same as in Fig. 13 for the distributions at 200 hPa.